Reference layer adaptive filtering (RLAF) for EEG artifact reduction in simultaneous EEG-fMRI

2017 J. Neural Eng. 14 026003

(http://iopscience.iop.org/1741-2552/14/2/026003)

OPEN ACCESS
IOP Publishing
Journal of Neural Engineering
J. Neural Eng. **14** (2017) 026003 (20pp)
doi:10.1088/1741-2552/14/2/026003

Reference layer adaptive filtering (RLAF) for EEG artifact reduction in simultaneous EEG-fMRI

David Steyrl[1,4], Gunther Krausz[2], Karl Koschutnig[3,4], Günter Edlinger[2] and Gernot R Müller-Putz[1,4]

[1] Laboratory of Brain-Computer Interfaces, Institute of Neural Engineering, Graz University of Technology, Graz, Austria
[2] GUGER TECHNOLOGIES OG, Graz, Austria
[3] Department of Psychology, University of Graz, Graz, Austria
[4] BioTechMed-Graz, Graz, Austria

E-mail: gernot.mueller@tugraz.at

Received 21 September 2016, revised 23 November 2016
Accepted for publication 25 November 2016
Published 3 February 2017

Abstract

Objective. Simultaneous electroencephalography (EEG) and functional magnetic resonance imaging (fMRI) combines advantages of both methods, namely high temporal resolution of EEG and high spatial resolution of fMRI. However, EEG quality is limited due to severe artifacts caused by fMRI scanners. *Approach.* To improve EEG data quality substantially, we introduce methods that use a reusable reference layer EEG cap prototype in combination with adaptive filtering. The first method, reference layer adaptive filtering (RLAF), uses adaptive filtering with reference layer artifact data to optimize artifact subtraction from EEG. In the second method, multi band reference layer adaptive filtering (MBRLAF), adaptive filtering is performed on bandwidth limited sub-bands of the EEG and the reference channels. *Main results.* The results suggests that RLAF outperforms the baseline method, average artifact subtraction, in all settings and also its direct predecessor, reference layer artifact subtraction (RLAS), in lower (<35 Hz) frequency ranges. MBRLAF is computationally more demanding than RLAF, but highly effective in all EEG frequency ranges. Effectivity is determined by visual inspection, as well as root-mean-square voltage reduction and power reduction of EEG provided that physiological EEG components such as occipital EEG alpha power and visual evoked potentials (VEP) are preserved. We demonstrate that both, RLAF and MBRLAF, improve VEP quality. For that, we calculate the mean-squared-distance of single trial VEP to the mean VEP and estimate single trial VEP classification accuracies. We found that the average mean-squared-distance is lowest and the average classification accuracy is highest after MBLAF. RLAF was second best. *Significance.* In conclusion, the results suggests that RLAF and MBRLAF are potentially very effective in improving EEG quality of simultaneous EEG-fMRI.

Highlights

- We present a new and reusable reference layer cap prototype for simultaneous EEG-fMRI
- We introduce new algorithms for reducing EEG artifacts due to simultaneous fMRI
- The algorithms combine a reference layer and adaptive filtering
- Several evaluation criteria suggest superior effectivity in terms of artifact reduction
- We demonstrate that physiological EEG components are preserved

Keywords: simultaneous EEG-fMRI, EEG artifact reduction, reference layer cap, adaptive filtering, reference layer adaptive filtering, multi band reference layer adaptive filtering

(Some figures may appear in colour only in the online journal)

Introduction

Electroencephalography (EEG) as well as functional magnetic resonance imaging (fMRI) are standard tools for non-invasive functional brain imaging (Michel and Murray 2012, Norris 2006). EEG captures electrical potentials at the scalp, whereas fMRI captures blood oxygenation level dependent (BOLD) signals in the brain (Ogawa *et al* 1990, Niedermeyer and Lopes da Silva 2005). These two techniques have complementary characteristics: EEG has a high temporal resolution in the range of milliseconds, while fMRI has a high spatial resolution in the range of millimeters and is also capable of measuring activity in deep brain regions (He *et al* 2011, Laufs 2012). Concurrent measurement of EEG and fMRI allows benefitting from the advantages of both methods (Huster *et al* 2012, Uludag and Roebroeck 2014). This combination is often termed as simultaneous EEG-fMRI (Ritter and Villringer 2006).

Several aspects of simultaneous EEG-fMRI, however, remain challenging (He *et al* 2011). One technical challenge is the existence of a complex mutual influence of these two methods, when applied simultaneously. On the one hand, EEG electrodes reduce static magnetic field homogeneity of MRI scanners, which in turn influences MRI signal quality negatively. MRI signal quality is worsened on the scalp and in the brain, however, the impact is negligible on the fMRI BOLD signal (Bonmassar *et al* 2001, Luo and Glover 2012). On the other hand, MRI scanners cause several serious artifacts in EEG signals during standby and during their operation. EEG artifacts due to simultaneous fMRI can in principle be reduced by adequate signal processing methods. The means for obtaining high quality EEG in simultaneous EEG-fMRI, however, are still an issue of ongoing research (Mulert and Lemieux 2010, Mullinger and Bowtell 2011). In this work, we present a new EEG cap in combination with new artifact reduction methods to improve EEG signal quality substantially. Before we go into details of our work, we recap EEG artifact characteristics and illustrate difficulties which hinder a straightforward artifact reduction.

(1) The most prominent artifact is the gradient artifact (GA). It is caused by induction in the leads of EEG electrodes due to magnetic field gradient switching during fMRI data acquisition (Allen *et al* 2000). The GA amplitudes are 2–3 orders of magnitude higher than the underlying EEG which masks the EEG completely (Allen *et al* 2000, Mullinger *et al* 2011). Analysis in the frequency domain reveals a coverage of the whole frequency range. An axial repositioning of study participants out of the MRI scanner's iso-center as well as an optimized routing of leads to minimize loops help to reduce the impact of the GA (Mullinger *et al* 2011, Jorge *et al* 2015a). However, signal processing based GA reduction is absolutely essential for achieving acceptable EEG signal quality. The most common GA reduction method is average artifact subtraction (AAS) (Allen *et al* 2000). It exploits the repetitive nature of the GA. For each EEG channel separately, EEG data are segmented into artefact epochs and subsequently, an artifact template is computed through averaging over artifact epochs. Finally, artifact templates are subtracted from each artifact epoch to unveil the underlying EEG signal. Synchronization of the EEG sampling with the MRI scanner clock ensures that the GA is always sampled at the same times per epoch and hence improves quality of artifact templates (Mullinger *et al* 2008). However, even a slight motion of the study participant alters the shape of the GA and therefore the template fit will be impaired. Hence, residuals of the GA with magnitudes in the range of EEG signals may occur even after AAS.

(2) After attenuating the GA or when the MRI scanner is not operating, a second EEG distortion is visible, the ballisto-cardiogram artefact or pulse artifact: an artifact in synchrony with the cardiac-pulse-cycle. To emphasize its coupling with the cardiac-pulse-cycle, we stick to the name pulse artifact (PA) throughout this work. The PA has two main causes: on the one hand, slight electrode motions in the static magnetic field, like cardiac-pulse-driven head rotations and local scalp motions due to the expansion and contraction of scalp arteries, and on the other hand, blood-flow induced Hall voltage (Bonmassar *et al* 2002, Mullinger *et al* 2013a). The contribution of the Hall effect to the PA, however, is small compared to the contribution of electrode motions (Mullinger *et al* 2013a). Amplitudes of the PA increase with field strength, making the artifact more problematic in modern MRI scanners with their very strong static magnetic fields of 3–7 T (Debener *et al* 2008, Mullinger *et al* 2013a). The PA can have amplitudes greater than 50 μV at 3 T and has its largest components in lower frequency ranges up to ~30 Hz (Allen *et al* 1998, Debener *et al* 2007, Debener *et al* 2008). AAS is again the most common method to tackle this artifact (Allen *et al* 1998). Simultaneously recorded electrocardiogram (ECG) data are used to find epochs of the PA in EEG. Separate PA templates are computed for each EEG channel and subsequently subtracted from PA epochs. However, the cardiac cycle inherently varies over time, and therefore the PA varies too, which in turn limits the success of the AAS method, since artifact templates only approximately fit the PA. Like with residuals of the GA, PA residuals are in the same order of magnitude as EEG signals. Moreover, PA residuals mask brain signals more profoundly than GA residuals since they are in the same frequency band as the brain signals.

(3) Another source of artifacts in the EEG of simultaneous EEG-fMRI is the helium pump of the coolant system of the MRI scanner (Mullinger *et al* 2013b, Nierhaus *et al* 2013). This helium pump artifact (HPA) has not been sufficiently studied yet. Its shape and strength varies and is heavily dependent on the MRI scanner itself (Nierhaus *et al* 2013, Rothlübbers *et al* 2014). In frequency domain analysis, the HPA shows several prominent peaks with amplitudes of up to ~1 μV Hz^{-1} ranging from ~45 Hz to ~55 Hz and from ~90 Hz to ~115 Hz. It is not yet popular to apply HPA reduction methods, although at least one method has been published (Rothlübbers *et al* 2014).

(4) The internal ventilation system of MRI scanners has recently been identified as an additional source of specific artifacts in the EEG (Nierhaus *et al* 2013). In frequency domain analysis, Nierhaus *et al* found prominent peaks at ~37 Hz and at ~42 Hz depending on the ventilation level of the MRI scanner. Amplitudes of up to 20 μV can occur (Nierhaus *et al* 2013). The exact shape of the ventilation artifact (VA) is most likely specific to a particular MR scanner make or model (Nierhaus *et al* 2013). To our knowledge, this artifact has not been well studied yet and therefore, no dedicated VA reduction method is available. Of course, it is possible to circumnavigate these two last mentioned artifact types (3, 4) by temporarily switching the helium pump and ventilation system off. However, this is not desirable, since these systems have important roles for a save operation of the MRI scanner and for the comfort of the study participant.

(5) The motions of study participants cause strong artifacts in the EEG due to Faraday's law of induction in the static magnetic field of the MRI scanner. Shape and amplitudes of motion artifacts (MA) are not predictable and can easily superimpose EEG signals (van der Meer *et al* 2010). Several methods to reduce this kind of artifacts have been proposed (Bonmassar *et al* 2002, Masterton *et al* 2007, van der Meer *et al* 2010, Abbott *et al* 2014, Jorge *et al* 2015b). Most of them attempt to capture MA separately to subsequently subtract them from EEG. The motions of study participants are problematic in two senses. First, they induce artifacts. Second, they also limit the success of artifact reduction methods based on the repetitiveness of artifacts, because their shape will change with the position of the study participants.

These very different artifact characteristics combined with the need for EEG quality improvements have pushed the development of a variety of artifact reduction methods over the past decade. Beside AAS, optimal basis sets (OBS) artifact reduction (Niazy *et al* 2005, Wu *et al* 2016) and independent component analysis artifact reduction are also popular at the present time (Srivastava *et al* 2005, Briselli *et al* 2006, Mantini *et al* 2007, Ritter *et al* 2007, Vanderperren *et al* 2010, Abreu *et al* 2016). Other methods, for example based on beam former, singular value decomposition, linear predictors, independent vector analysis and dictionary learning, have been published and can outperform popular methods under certain conditions (Brookes *et al* 2008, Liu *et al* 2012, Ferdowsi *et al* 2013, Abolghasemi and Ferdowsi 2015, Acharjee *et al* 2015). Generally, each method has its merits and caveats and an optimal choice is tricky. Preferably, one would like to have a method at hand that reduces as many as possible of the aforementioned artifacts in one step.

Chowdhury *et al* published new investigations on a very promising approach that was invented by a no longer existing company named Alatheia Ltd (Chantilly, VA, USA) in their 'fEEG' system (Dunseath *et al* 2009, McGlone *et al* 2009, Chowdhury *et al* 2014). This approach is conceptually able to tackle all occurring artifacts at once. The idea is to capture all kinds of artifacts at the head at once and subtract them from the EEG. Chowdhury *et al* used agar and PVC film to build a reference layer for the head, which is electrically isolated from the scalp, but has similar electrical properties and shape. They used electrode pairs, where one electrode is capturing the artifact afflicted EEG at the scalp (scalp electrode), while the other is capturing artifacts at the reference layer (reference electrode). Electrodes of a pair are closely spaced, reference electrodes on top of scalp electrodes, separated by PVC film only. Hence, it can be assumed that artifacts captured by an electrode pair are similar and a subsequent subtraction of artifacts from the artifact afflicted EEG unveils the underlying true EEG. Since this approach makes use of a reference layer and subsequent artifact subtraction it is termed as reference layer artifact subtraction (RLAS). Generally, RLAS can effectively attenuate all kinds of artifacts that are captured by reference electrodes. It was demonstrated that RLAS outperforms AAS in terms of GA and PA attenuation when MA are present (~1 dB lower root-mean-square (RMS) voltages) and that RLAS is even more effective when combined with AAS as pre-processing step (min. ~7 dB lower RMS voltages) (Chowdhury *et al* 2014).

We identified two components of the RLAS approach that can be optimized. First, the reference layer itself was cumbersome, unstable and not reusable. Chowdhury *et al* concluded that for broader use, '*…it will be necessary to devise a more robust reference layer arrangement that is also easier to use…*' (Chowdhury *et al* 2014). Second, artifacts captured by electrode pairs are similar, but not equal, because of the following reasons: (i) electrodes of a pair cannot be positioned at the exact same place, (ii) electrodes of a pair can move differently, since they are not mechanically coupled, (iii) the shape of the reference layer cannot be totally equal to the shape of the head of course, and (iv) impedances of electrode pairs can differ. Consequently, residuals are present after artifact subtraction. However, due to Faraday's law of induction, it is valid to assume a linear relationship between artifacts captured at the reference layer and artifacts captured at the scalp, but the relationship can change over time, since for example the impedances can change (Yan *et al* 2010, Jorge *et al* 2015b). Adaptive filters, correctly applied, find an optimal scaling for the artifact to subtract and adapt the scaling over time to meet the optimization criterion (Haykin 1986).

Hence, we introduce a new reference layer cap prototype and present artifact reduction methods that replace the subtraction of the original RLAS approach with adaptive filtering. We name this approach reference layer adaptive filtering (RLAF).

We also incorporate ideas of other groups, but our approach is substantially different to already published methods. (i) In contrast to Xia *et al*, Luo *et al*, Chowdhury *et al*, we filter electrode pair signals adaptively (Xia *et al* 2013, Chowdhury *et al* 2014, Luo *et al* 2014). Hence, reference layer electrode signals are not only just subtracted from scalp electrode signals, but are adaptively scaled before subtraction. (ii) We introduce a new, truly reusable reference layer cap prototype, which is equipped with mechanically tightly coupled and narrow spaced electrode pairs. The coupling ensures that electrodes of a pair can only move together, meaning that all electrode motion related artifacts are equally captured by both electrodes. This is in contrast to Masterton *et al*, Xia *et al*, Luo *et al*, Jorge *et al* and van der Meer *et al*, where reference electrodes are able to move independently of the scalp electrodes due to their separate placing (Masterton *et al* 2007, Xia *et al* 2013, Luo *et al* 2014, Jorge *et al* 2015b, van der Meer *et al* 2016). (iii) the electrode pairs of our cap provide reference electrode signals without occupying scalp electrode positions, hence all EEG positions are available to enable high density EEG recording. In Xia *et al*, Luo *et al* and Jorge *et al* electrodes occupy scalp electrode positions (Xia *et al* 2013, Luo *et al* 2014, Jorge *et al* 2015b). (iv) The electrode pairs provide a dedicated reference electrode signal per scalp electrode and avoid a reference signal construction that is based on the assumption that individual reference signals can be calculated by a linear combination of a few distributed reference electrode signals, as assumed in Xia *et al* (2013), Luo *et al* (2014), Jorge *et al* (2015b) and van der Meer *et al* (2016).

We already presented a proof-of-concept of our RLAF approach with a spherical fMRI phantom in Steyrl *et al* (2015). Within this work, we present details on the reference layer cap prototype. We show that adaptive filtering instead of subtraction potentially improves the reference layer approach. We evaluate the RLAF artifact reduction method on simultaneous EEG-fMRI data of humans with regard to EEG data quality enhancement. For this purpose we show time courses of the EEG after artifact reduction methods, we analyze EEG root-mean-square voltage changes and EEG power reduction, we demonstrate that both, evoked and induced EEG activity are preserved, and that single-trial quality of event related potentials is improved. We compare our RLAF results with its direct predecessor RLAS and with the most common artifact reduction method AAS. And finally, we present a new extension of the RLAF approach named multi band reference layer adaptive filtering (MBRLAF), which performs adaptive filtering on bandwidth limited sub-bands of the EEG and the reference channels to potentially improve RLAF further.

Materials and methods

Participants

Two volunteers (both female, 25 and 23 years old) participated in this experiment which was performed in accordance with the Declaration of Helsinki and was approved by the local ethics committee. Participants had medical histories free of neurological problems and were not under medication. They were fully informed about the objectives of the experiment and gave consent for participation before taking part.

Experiment description

The experiment was designed to evaluate evoked responses (visual evoked responses) and induced responses (alpha-rhythm changes). After EEG cap setup and instructions the participants lay in the MRI scanner, while looking at a monitor via a head coil mounted mirror. The monitor was positioned at the foot end of the scanner. The participants were asked to remain as still as possible during the experiment. In the first part of the experiment, the participants underwent inverse checkerboard stimuli to trigger visual evoked potentials (VEP). The checkerboard had 8×8 square black and white fields with a centered red dot, was scaled to the size of the monitor and was inverted after a randomized duration of 0.5s–0.6s. EEG data of 1200 inversions were collected, which lasted approximately 11 min. In the second part, 10 min of resting EEG was recorded to allow analysis of induced activity changes between eyes open and eyes closed. The participants were instructed to close their eyes, but not to fall asleep. The total duration of the experiment was approximately 70 min, including 40 min cap preparation and instructions, 20 min measurement, 10 min additional time for handling.

Reference layer cap prototype

The reference layer cap used in this study was a prototype developed by GUGER TECHNOLOGIES OG, Austria (patents pending), see figure 1 panel A and B. It consists of 30 double-layer electrode pairs and 2 additional ECG electrodes. Twenty-nine electrode pairs for capturing EEG and one electrode pair as common ground/reference electrode. Each electrode has two C-shaped silver-coated contact areas with a diameter of 2.5 mm. The electrode contacts of each electrode are placed on both sides of a corresponding printed circuit board (PCB) with a thickness of 1 mm and a diameter of 9 mm. The PCBs are mounted into isolating plastic electrode housings which are sealed with epoxy resin. The plastic housings have a diameter of approximately 14 mm and are approximately 8 mm thick. The inner electrode contacts connect to the subject's scalp via conductive electrode gel (scalp layer) and the outer electrode contacts connect to a grid made of silicone tubes which is filled with physiological saline solution (reference layer). For a schematic representation of an electrode see figure 1 panel C. The reference layer is galvanically isolated from the scalp layer, only at the common ground/reference electrode both layers are galvanically connected to each other, see figure 1 panel C and D. All electrode contacts (scalp layer and reference layer) are equipped with 5 kΩ non-magnetic current limiting resistors which are built in the electrodes. Wire pairs run from each electrode pair to a coupling board allowing the connection of the cap to the EEG recording system. Each wire at the coupling board is also equipped with a 5 kΩ current limiting resistor. The distance between the coupling board and the cap is about 50 cm (see figure 1 panel B). Two additional leads run from the coupling board to the cap

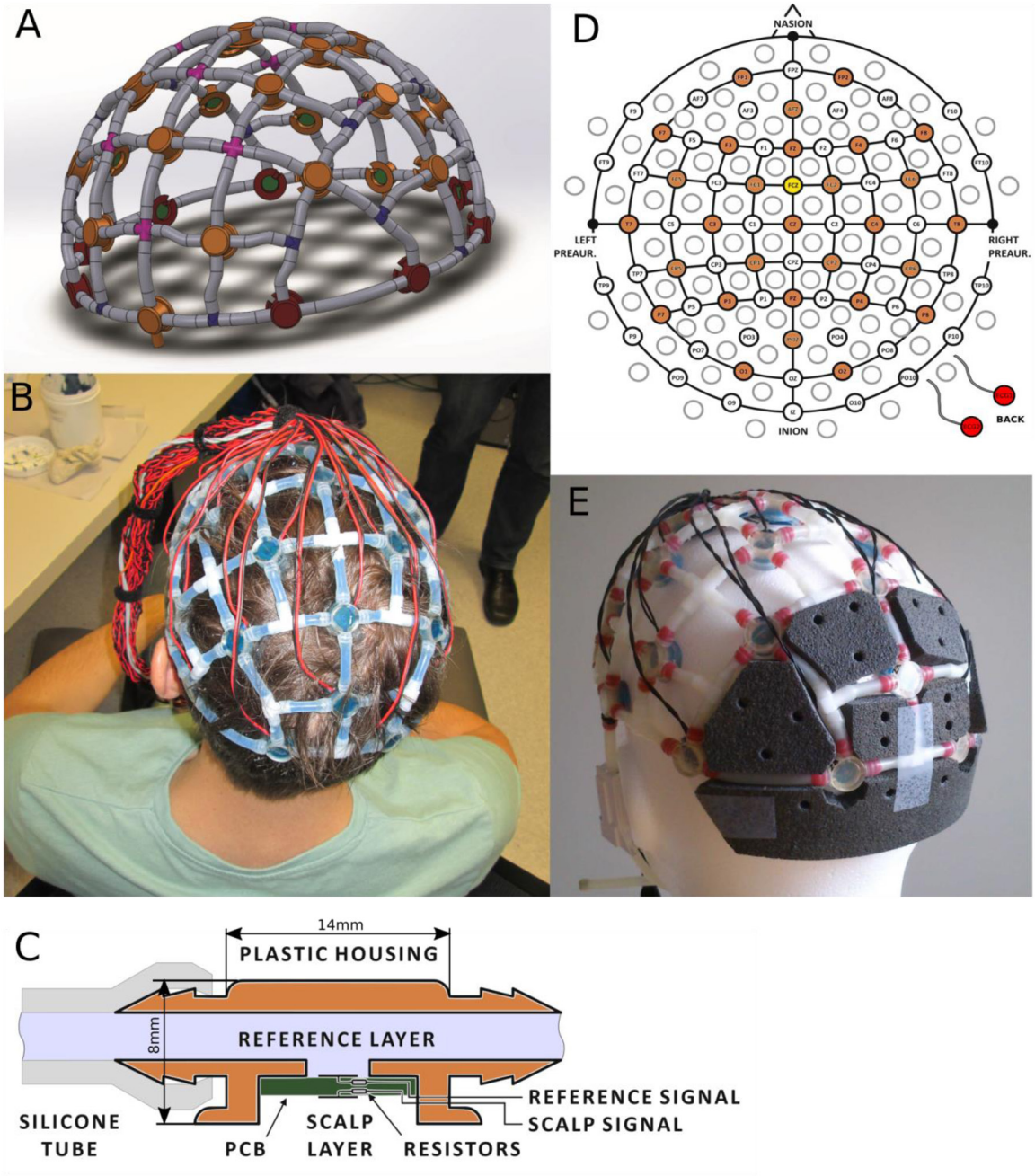

Figure 1. Reference layer cap prototype. Panel A: rendering of the reference layer cap prototype. Panel B: actual cap with cabling. Panel C: principle of a reference layer electrode pair. Panel D: cap layout with electrode positions in the extended 10/20 system. The common ground/reference electrode is colored yellow. The ECG electrodes are colored red. Panel E: cap equipped with foam pads for comfort.

and down to the back of study participants to connect to two self-adhesive MRI compatible ECG electrodes (see figure 1 panel D). The complete positioning of electrodes according to the international extended 10/20 system is shown at figure 1 panel D. To prevent pain resulting from head weight resting on a few electrodes, we putted foam pads in between of the occipital electrodes to distribute the weight, see figure 1 panel E. Temperature measurements were conducted before the cap was used on human. The cap was mounted on a spherical, electrode gel covered fMRI phantom. fMRI compatible heat sensors measured the temperature directly in the connecting gel between phantom surface and electrode. No heating above 1 °C was found during SAR intensive sequences. Hence, we consider the construction as safe concerning the heating due to the switching magnetic fields.

fMRI scanner and EEG recording system

Functional MRI data were acquired on a Siemens Skyra 3.0 T (Siemens, Erlangen, Germany) at the MRI-Lab Graz (Austria) using a 20 channel head coil. The helium pump was active, ventilation was set to lowest level possible. A standard EPI sequence was implemented (TR = 2000 ms, TE = 24 ms, base resolution = 64, 3.5 × 3.5 × 3.5 mm³ voxel size, no gap,

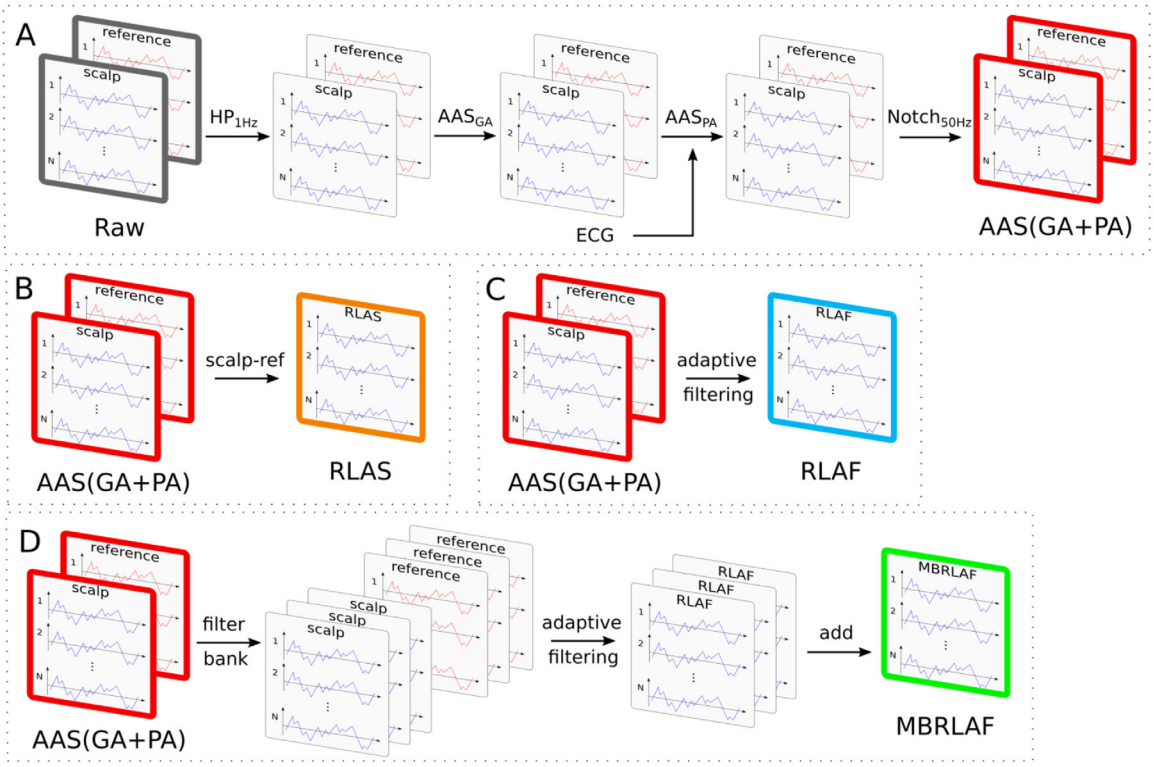

Figure 2. Signal processing chain. Panel A: the pre-processing chain included high pass filtering (HP), average artifact subtraction (AAS) of the gradient artifact (GA), AAS of the pulse artifact (PA) with support of electrocardiogram (ECG) data and notch filtering. Panel B: in RLAS, reference channels were subtracted of scalp channels. Panel C: in RLAF, reference channels were adaptively scaled before being subtracted from the scalp channels. Panel D: in MBRLAF, reference channels and scalp channels were decomposed into frequency components by a filter band. Reference channel components were adaptively scaled and subsequently subtracted of respective scalp channel components. Full bandwidth MBRLAF data were recomposed by adding up filtered components.

34 slices, field of view = 224 × 224). The fMRI data are not reported in this work.

EEG and ECG were recorded with a 64 channel MRI compatible EEG system (BrainAmp MR plus, Brain Products GmbH, Gilching, Germany). The EEG amplifier was positioned inside the borehole at the head end of the scanner on a wooden panel. Cables and amplifier were fixed with sand bags. All settings of the amplifier were according the manufacturer's recommendations. The sampling rate was 5 kHz, cutoff frequency of the hardware high pass filter was set to 0.016 Hz and cut off frequency of the hardware low pass filter to 250 Hz. The voltage range was ± 16.384 mV, resulting in a resolution of 0.5 μV/bit. The EEG system clock was synchronized with the gradient clock of the MRI scanner via the Brain Products SyncBox device to ensure a highly accurate GA sampling. Sync status was monitored. BrainVision Recorder (Brain Products GmbH, Gilching, Germany) software version 1.20.0802 was used for data recording. All data processing was performed offline, after the recording.

EEG data preprocessing

All 29 possible electrode pairs of the reference layer cap were recorded for each participant, but one pair of participant 1 (position Cz) and two pairs of participant 2 (position FC6 and CP2) had to be rejected due to electrode lift off during the experiment. Hence, signals of 55 of the 58 electrode pairs were taken for further analysis. In line with Chowdhury *et al* and Jorge *et al* but also due to our own pre-analysis, AAS was used as pre-processing step to reference layer methods (Chowdhury *et al* 2014, Jorge *et al* 2015b). Pre-processing was carried out offline for each electrode signal separately using BrainVision Analyser software (Brain Products GmbH, Gilching, Germany) version 2.1.1.327 and MATLAB (Mathworks Inc., Natick, MA, USA) version 2012b. Figure 2 panel A presents a schematic overview on the pre-processing. Pre-processing included the following steps: (i) Signal offsets were removed by applying a high pass filter (Butterworth zero phase) with a cut-off of 1 Hz and 48 dB/oct damping. (ii) The next step was GA reduction with AAS as implemented in BrainVision Analyser. During data recording the MRI scanner was sending markers whenever a new volume and hence a new GA started. These markers were used to divide the signal into GA epochs. A sliding average artifact template approach was chosen, which calculated GA templates separately for each epoch from 100 adjacent artifact epochs, 50 before and 50 after. This approach can be beneficial if slight changes in the artifact epochs occur. GA templates were subsequently subtracted from signals and all signals were down sampled to 250 Hz. (iii) PA reduction, the third step, was carried out with AAS as implemented in BrainVision Analyser software. The software supports a semiautomatic mode, where *R*-peaks are detected automatically in dedicated ECG recordings, manually adjusted and then used to divide

the signals into PA epochs. Like in the GA reduction step, a dedicated template for subtraction was computed for each PA epoch separately. A sliding window with 50 adjacent PA epochs, 25 epochs before and 25 epochs after each PA, was taken for calculating PA templates, which were subsequently subtracted. (iv) As the last step in pre-processing the data were exported to MATLAB and a 50 Hz notch filter (0.5 Hz bandwidth, 8th order, IIR) was applied. After preprocessing one reference channel and one EEG channel per electrode pair was left.

Reference layer artifact subtraction (RLAS)

After pre-processing, reference electrode signals were subtracted sample-by-sample from scalp electrode signals, separately for each electrode pair as in Chowdhury *et al* (2014). Hence, after RLAS, one EEG channel per electrode pair was left, see figure 2 panel B.

Reference layer adaptive filtering (RLAF)

In RLAF, artifact subtraction was replaced by adaptive filtering. Each electrode pair was treated separately and was thus filtered with its own adaptive filter. Respective reference electrode signals and scalp electrode signals were fed into first order least-mean-square (LMS) adaptive filters (Haykin 1986). The least-mean-square algorithm was chosen since it is the most common. The first order model restricted the adaptive filters to act like adaptive scalers. One can interpret this process as scaling of the artifact until the residual after subtraction has minimum power (Haykin 1986). The adaptation rate, which is the maximum change in scaling per step, is a crucial parameter. On the one hand, a restricted, thus small adaption rate prevents overfitting, because the filter cannot follow changes in signals instantly. On the other hand, we want the adaptive filter to follow changes in the scaling, this is why we use adaptive filters. Further, the adaptation rate is crucial to guarantee a stable adaptation process. Small adaptation rates increase the stability, whereas high adaptations rates can lead to unstable behavior. We calculated an individual adaptation rate for each adaptive filter. We thus multiplied the maximum value of the reference electrode signal with the maximum value of the skin electrode signal and multiplied this value by 10 for reducing residual errors and for improving stability. The inverse of this value was our adaptation rate and was between 7×10^{-6} and 1.5×10^{-4}, depending on the respective electrode pair. These small adaptation rates reduce the risk of overfitting the data. The actual adaptive filtering was performed in double pass. First, adaptive filtering was performed forward in time from beginning of the data to end of the data with initial scaling values of one. In a second pass, the scaling was initialized with final values of pass one and the adaptive signal filtering was performed backwards on the original unfiltered data. This procedure yielded a cleaner estimation of the scaling during the starting period, where the adaptive filter had not converged yet and was also used by Jorge *et al* (2015b). After RLAF, one EEG channel per electrode pair was left, see figure 2 panel C.

Multi band reference layer adaptive filtering (MBRLAF)

EEG power spectral density is known for an $1/f$ characteristic, hence, most of the power is found in low frequencies. Adaptive filters minimize total signal power after subtracting filtered reference signals from signals of interest. In case of the RLAF approach, adaptive filters minimized signal power after subtracting scaled reference signals from skin electrode signals. Thus the scalings of the reference signals were particularly fitted to low frequencies and not high frequencies. With MBRLAF, we present an improved version of RLAF which is not afflicted by that problem. In MBRLAF, adaptive filtering was not performed on the full bandwidth signal, but on bandwidth limited sub-bands of the reference and skin electrode signals (Shynk 1992). The full bandwidth signal was afterwards recomposed by adding up the adaptively filtered sub-band signals, see figure 2 panel D. MBRLAF included the following processing steps: (i) A filterbank decomposed reference electrode signal and skin electrode signal of each electrode pair into bandwidth limited sub-bands. (ii) Adaptive filtering was performed on each pair of sub-bands of reference and skin electrode signals separately. (iii) The adaptively filtered sub-band signals were added up to regain the final full bandwidth signal. In this work, we decomposed the full band spectrum into the following frequency sub-bands: from 1–16 Hz in 3 Hz broad bands and separate bands at 16–27 Hz, 27–39 Hz, 39–49.5 Hz, 49.5–50.5 Hz, 50.5–65 Hz, 65–75 Hz, 75–90 Hz and a final band at 90–120 Hz. The choice of the filter bands was motivated by the different artifact types described in the literature and visible in the signal spectra. The sub-bands are different from classical EEG bands, since we tried to define individual frequency bands for artifacts. The actual adaptive filtering was carried out in two passes, as described in the RLAF paragraph above. After MBRLAF, one EEG channel per electrode pair was left, see figure 2 panel D.

Analysis and performance metrics

In order to evaluate the RLAF and the MBRLAF approach on human EEG data, we used a procedure similar to Jorge *et al* (2015b) and included the following analyses: (i) comparison of time courses of EEG signals after artifact reduction, (ii) scaling factors of the adaptive filters, (iii) root-mean-square (RMS) voltage changes, (iv) power spectra (ratio) changes and (v) single trial VEP quality before and after artifact reduction.

Nothing can substitute a direct inspection of the EEG signals. We show a representative example of EEG time courses after applying artifact reduction methods. This specific example was chosen because it shows alpha-rhythm activity and is also afflicted by artifacts. It was taken from the eyes closed part of participant 1 at position O_2, starting 760s after the beginning of the experiment and lasts 8s.

We present scaling factors of the adaptive filters captured at half time during the forward pass to illustrate the necessity of a scaling of the reference signal before subtraction. The choice of time was arbitrary, but motivated by the idea to report representative scaling values. Further we show selected time courses of the scaling factors of adaptive filters for

representative channels over the total signal length. Changes in the scaling factors over time indicate that a onetime fit is insufficient. Scaling values different from one indicate that a straight subtraction is not optimal.

EEG RMS voltages before and after artifact reduction quantify artifact attenuation, under the condition that EEG components are preserved. EEG RMS voltage reduction is then a measure of artifact magnitude that actually was subtracted. The data of the entire experimental time course were used to calculate RMS voltages. The computation was performed separately for each EEG channel of each participant before and after applying different artifact reduction methods. Starting from these RMS voltages per channel, two measures were calculated. (i) Average RMS voltages were computed over EEG channels, hence, an average RMS voltage for raw EEG data and an average RMS voltage per artifact attenuation method. Reductions of these average RMS voltages were calculated relative to the Raw EEG in percent of Raw EEG. (ii) Per channel RMS voltage reduction were calculated in dB relative to raw EEG for each artifact reduction method separately by

$$\text{attenuation}_{\text{dB}} = 20 \cdot \log_{10}\left(\frac{\text{RMS}_\text{i}}{\text{RMS}_\text{f}}\right), \tag{1}$$

with RMS_i being the RMS voltage after artifact attenuation and RMS_f before (Raw) artifact attenuation. We report median and min/max values of these per channel reductions.

EEG is traditionally analyzed in frequency bands. These bands were classically associated with task specific changes in their power. Hence, an analysis of artifact attenuation per frequency band is of interest. The full band EEG data were decomposed into the most common frequency bands: delta (1–4 Hz), theta (4–8 Hz), alpha (8–13 Hz), beta (13–30 Hz), and gamma (30–120 Hz). These frequency bands defined 3 dB cut-off frequencies of five 12th order second-order IIR band pass filters with zero phase. The average power of frequency bands was calculated by squaring and subsequently averaging each frequency band separately over the full experimental time course of EEG channels. Hence separate band power values per method and frequency band were computed. We report the average band power over channels and the reduction in average band power relative to Raw EEG in dB. Lower power implies lower artifacts under the condition of preserved physiological EEG components.

It is known that a high spatial quality of EEG signatures is hard to obtain in simultaneous EEG-fMRI measurements. Several inside scanner artifacts are harder to deal with at lateral electrodes positions than at central positions. We show alpha power topographies during eyes closed after applying different artifact reduction methods. Better performing artifact reduction methods should show a more dipolar topography. In particular, homogeneous and low alpha power in frontal and central electrode positions and high alpha power at occipital electrode positions.

Full spectrum visualization gives a more detailed view on how well artifact attenuation methods suppress artifacts with specific spectral fingerprints. A Welch power spectral density estimation approach was applied to EEG data of the full experimental time course. The EEG data were segmented into windows with a length of 5s and an overlap of 631 samples (~50% overlap). A 1250 point fast Fourier transformations (FFT) was applied to each window and averaged over windows. Spectra were subsequently averaged over EEG channels, leading to separate average power spectra for each method.

To illustrate that reference layer based approaches preserve task specific induced EEG activity, we calculated separate spectra of eyes closed and eyes open tasks after AAS and MBRLAF, averaged over occipital channels O1, O2, POZ, P3, P4, and PZ. The procedure of spectra estimation was the same as described in the paragraph above. Further we calculated ratios of power in alpha band between eyes closed and eyes open for occipital channels O1, O2, POZ, P9, P3, PZ, PZ, P4, and P8 with

$$\text{alpha power ratio} = \frac{P_{\alpha\text{c}}}{P_{\alpha\text{o}}}, \tag{2}$$

were $P_{\alpha\text{c}}$ is the average power in alpha band during eyes closed and $P_{\alpha\text{o}}$ is the average power in alpha band during eyes open. This ratio becomes higher when less noise is in the data and becomes lower when alpha power at eyes closed in removed.

To show that reference layer methods preserve evoked brain activity, we calculated separate average visual evoked responses per artifact reduction method. Before averaging a band pass filter (0.5–10 Hz bandwidth, 12th order, SOS-IIR, zero phase) was applied. We collected data of 1200 repetitions of the VEPs during the first part of our measurements. This high number allows for an accurate estimate of the true VEP, even when the artifact reduction methods are not perfect. Hence, VEPs after different artifact reduction methods should be very similar. Differences in average VEPs implies a removal of evoked responses of the respective method. In addition to check for evoked activity preservation, we used VEP homogeneity as a quality measure for artifact reduction methods, similar to Vanderperren *et al* (2010). Of course, VEPs are as a rule intrinsically variable, but if an artifact attenuation method can reduce the variability and thus increase the homogeneity of the VEPs without changing the average VEP, this then means that the method removes artifacts. To quantify VEP homogeneity, mean-squared-distances (MSD) of single VEP epochs to their corresponding average VEP were calculated before and after artifact attenuation methods were applied. Another VEP quality measure is single trial VEP classification accuracy. Equal classification accuracies indicate that physiological components, hence, the information in the EEG, were preserved. Higher classification accuracies indicate that the signal-to-noise ratio was improved. To estimate single trial classification accuracy, 100 repetitions of 5-fold cross-validations were performed. Analytical shrinkage regularized linear discriminant analysis (sLDA) was the classifier of choice (Blankertz *et al* 2011). The dataset consisted of 2 classes. Class 1 were 1200 VEPs measured at skin electrodes O1 and O2. Class 2 were 1200 windows with equal length as the VEPs also measured at skin electrodes O1 and O2, but drawn from random positions in time of the eyes closed part

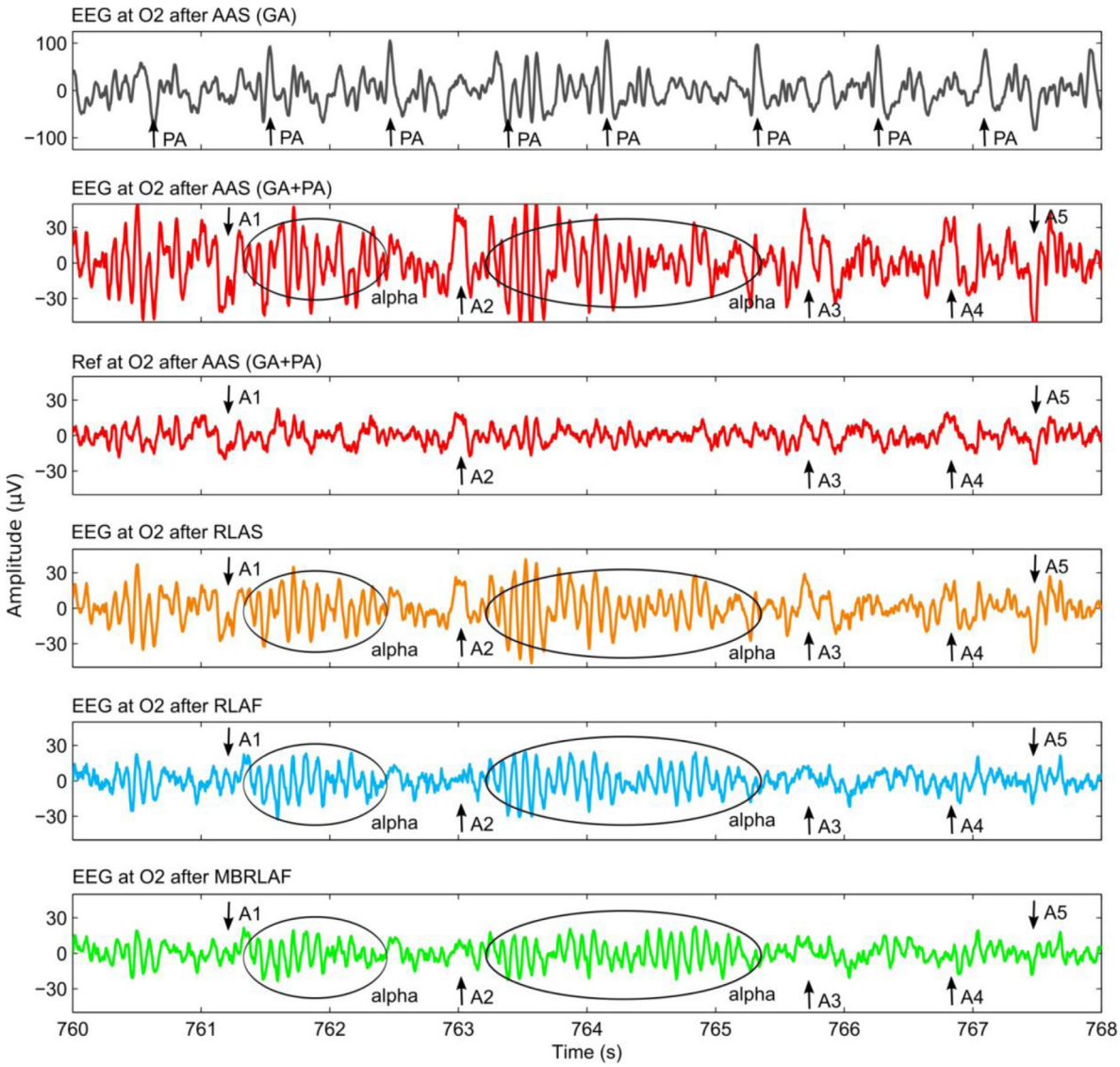

Figure 3. Representative example of EEG time courses after applying artifact reduction methods. The example is taken from channel O_2 and the corresponding reference channel (Ref) of participant 1 starting 760s after the beginning of the experiment. The participant had her eyes closed. Arrows PA mark pulse artifacts. Arrows A1 to A5 mark artifact positions. Be aware of the different scaling of the first row. Artifact reduction methods: average artifact subtraction of gradient artifact and pulse artifact (AAS of GA + PA), reference layer artifact subtraction (RLAS), reference layer adaptive filtering (RLAF), and multi band reference layer adaptive filtering (MBRLAF).

of the experiment. These class 2 data were redrawn for each repetition of the cross-validation process to not be susceptible to random variations in classification results caused by the choice of class 2 data.

Results

Figure 3 shows an eight second piece of EEG of channel O_2 of participant 1 after applying artifact reduction methods and in addition the according reference channel. The EEG piece is taken from the eyes closed part of the experiment where we anticipate increased alpha-rhythm activity. EEG after AAS of the gradient artifact is superimposed by very prominent pulse artifacts. The PAs are marked with an arrow in figure 3 top row. The repetitive nature of the PA is clearly visible with a frequency of ~1.1 Hz, which corresponds to a pulse rate of ~66. Comparing the shape of the 1st and 2nd PA, one can recognize the PAs intrinsic variability. It is hardly possible to identify other artifacts or physiological components like alpha-rhythm. After AAS of the pulse artifact, the PA is not visible anymore in our EEG example and alpha-rhythm activity became recognizable. However, also artifacts became visible and are marked with arrows (A1 to A5) in figure 3 second row. The aforementioned artifacts (A1 to A5) are also visible in the corresponding reference channel, which is mandatory for a successful application of RLAS, RLAF, or MBRLAF. The reference channel after AAS of the GA and the PA is depicted in figure 3 third row. After RLAS, amplitudes of the EEG are generally smaller compared to the amplitudes after AAS (GA + PA), because the reference channel was subtracted. Alpha-rhythm activity is clearly visible. Although the artifacts A1 to A5 are smaller after RLAS than after AAS (GA + PA), they are still present. Figure 3 fourth row shows the EEG after RLAS.

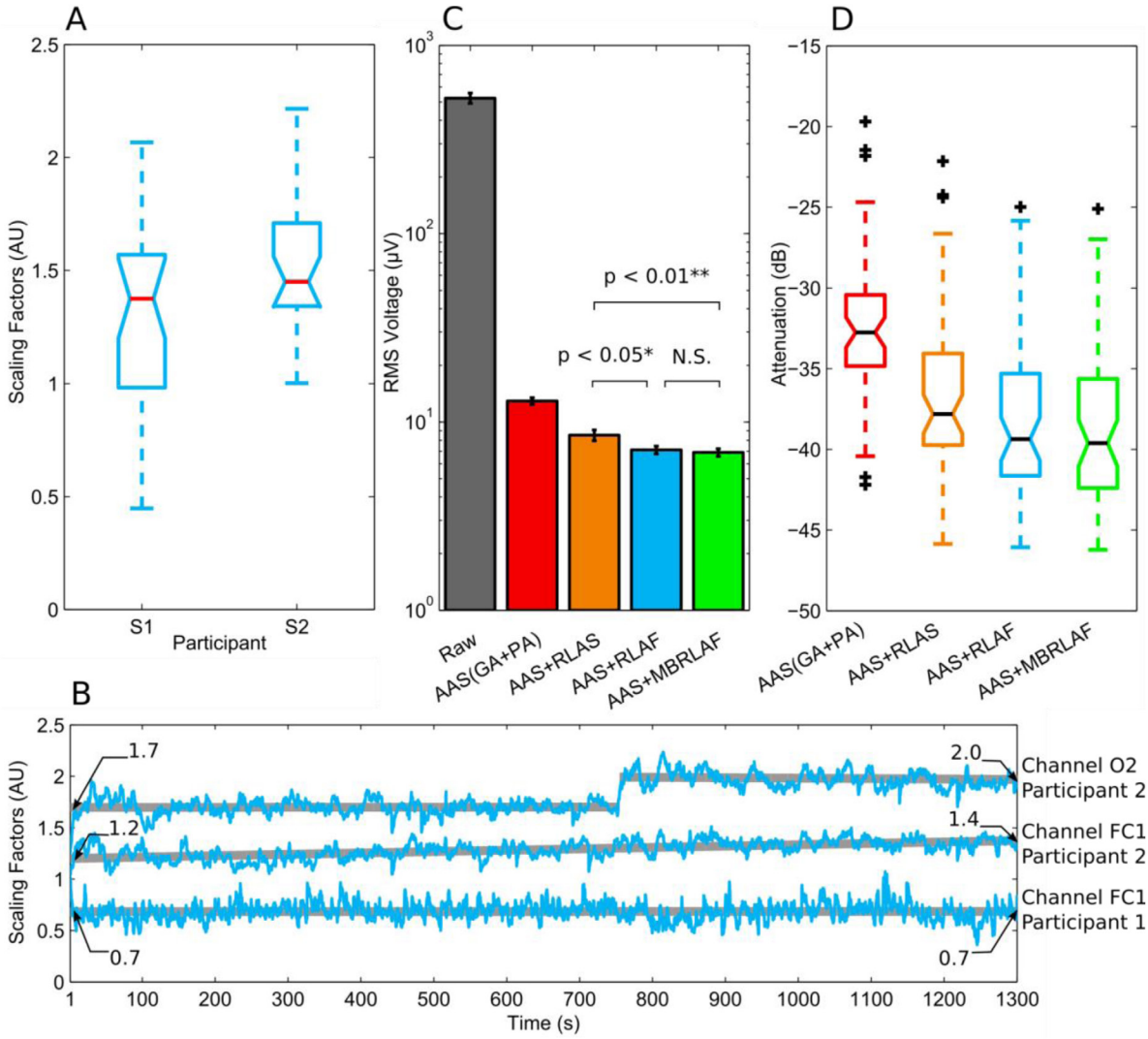

Figure 4. Scaling factors of adaptive filters after the half experiment duration (A), examples of time courses of adaptive filter scaling factors (B), root-mean-square (RMS) voltages after different artifact reduction methods (C), and attenuation by artifact reduction methods (D). A: panel A shows scaling factors of all channels for RLAF at halftime of the experiment. B: panel B shows examples of time courses of adaptive filter scaling factors in RLAF. The examples are taken from channels O_2 and FC1 of participant 2 and from channel FC1 of participant 1. The grey lines represent linear fits to the scaling factors. C: panel C shows average RMS EEG voltages. The average was computed over both participants' total experimental data of skin electrode signals before (Raw) and after artifact reduction. The error bars indicate standard error of the mean. D: panel D shows the boxplot of RMS voltages after artifact attenuation relative to Raw RMS voltages of skin electrodes in dB. Artifact reduction methods: average artifact subtraction of gradient artifact and pulse artifact (AAS of GA + PA), reference layer artifact subtraction (RLAS), reference layer adaptive filtering (RLAF), and multi band reference layer adaptive filtering (MBRLAF).

After RLAF, amplitudes are even smaller than after RLAS and after AAS (GA + PA), because the reference channel was scaled before subtraction. This scaling has direct impact on the aforementioned artifacts A1 to A5. They are greatly reduced und appear hardly visible. Alpha-rhythm activity is still clearly visible. Figure 3 fifth row displays the EEG after RLAF. After MBRLAF, amplitudes are again generally smaller than after RLAF, RLAS, or after AAS (GA + PA), since the adaptive scaling is now fitted per frequency band. Therefore, the fit of the reference channel to the EEG channel is better, which in turn leads to the smaller amplitudes after subtraction. Like after RLAF, the residuals of the artifacts A1 to A5 are small and hardly recognizable. Alpha-rhythm activity is clearly visible. See figure 3 last row for the EEG after MBRLAF.

The scaling factors of adaptive filters, which give a clue on the necessity of scaling the reference channels before subtracting them from EEG channels, were in median 1.38 and 1.45 for participant 1 and participant 2, respectively, after half time of the experiment. For participant 1 the minimum and the maximum scaling factor was 0.45 and 2.07, respectively. For participant 2 the minimum and the maximum scaling factor was 1 and 2.22, respectively. See figure 4 panel A for a boxplot of the scaling factors of all channels at half time of the experiment. Adaptive filters can change the scaling factors over time if necessary. We perceived the following three types of adapting the scaling factors: (i) merely slight or no changes over time. (ii) Steadily increasing or decreasing scaling factors. (iii) Sudden, abrupt changes in scaling factors. Examples for each of these behaviors are given is figure 4 panel B.

Table 1. Average RMS voltage over the experiment duration and channels in μV of Raw EEG and after applying artifact reduction methods. RMS voltage reduction in % relative to Raw EEG and relative to artifact reduction methods: average artifact subtraction of gradient artifact and pulse artifact (AAS of GA + PA), reference layer artifact subtraction (RLAS), reference layer adaptive filtering (RLAF), and multi band reference layer adaptive filtering (MBRLAF).

	RMS voltage (μV)	Reduction to Raw EEG	Reduction to AAS(GA + PA)	Reduction to AAS + RLAS	Reduction to AAS + RLAF
Raw EEG	524	—	—	—	—
AAS(GA + PA)	12.9	−97.5%	—	—	—
AAS + RLAS	8.5	−98.4%	−34.1%	—	—
AAS + RLAF	7.1	−98.6%	−45.0%	−16.5%	—
AAS + MBRLAF	6.9	−98.7%	−46.5%	−18.8%	−2.8%

Table 2. Median RMS voltage reduction over channels per method relative to Raw EEG in dB. Minimum and maximum RMS voltage reduction over channels per method relative to Raw EEG in dB. Artifact reduction methods: average artifact subtraction of gradient artifact and pulse artifact (AAS of GA + PA), reference layer artifact subtraction (RLAS), reference layer adaptive filtering (RLAF), and multi band reference layer adaptive filtering (MBRLAF).

Method	Median RMS voltage reduction over ch (dB)	Min RMS voltage reduction at a ch (dB)	Max RMS voltage reduction at a ch (dB)
AAS	−32.7	−19.7	−42.2
AAS + RLAS	−37.8	−22.2	−45.8
AAS + RLAF	−39.4	−25.0	−46.0
AAS + MBRLAF	−39.6	−25.1	−46.2

Table 3. Absolute (μV^2) average power over channels in frequency bands before (Raw) and after applying artifact reduction methods. Reduction in average power per frequency band relative to Raw power in dB. Artifact reduction methods: average artifact subtraction of gradient artifact and pulse artifact (AAS of GA + PA), reference layer artifact subtraction (RLAS), reference layer adaptive filtering (RLAF), and multi band reference layer adaptive filtering (MBRLAF).

Method	*P* in delta/red. to Raw	*P* in theta/red. to Raw	*P* in alpha/red. to Raw	*P* in beta/red. to Raw	*P* in gamma/red. to Raw
Raw	299.6 μV^2/0 dB	462.9 μV^2/0 dB	651.6 μV^2/0 dB	11 736.4 μV^2/0 dB	318 343.5 μV^2/0 dB
AAS	67.3 μV^2/−13.0 dB	33.0 μV^2/−22.9 dB	30.6 μV^2/−26.6 dB	12.8 μV^2/−59.2 dB	5.7 μV^2/−94.9 dB
AAS + RLAS	40.4 μV^2/−17.4 dB	10.7 μV^2/−32.7 dB	12.8 μV^2/−34.1 dB	6.3 μV^2/−65.4 dB	2.8 μV^2/−101.1 dB
AAS + RLAF	21.2 μV^2/−23.0 dB	6.9 μV^2/−36.5 dB	8.6 μV^2/−37.6 dB	5.2 μV^2/−67.1 dB	3.2 μV^2/−100.0 dB
AAS + MBRLAF	21.2 μV^2/−23.0 dB	6.5 μV^2/−37.1 dB	7.2 μV^2/−39.1 dB	4.9 μV^2/−67.6 dB	2.7 μV^2/−101.4 dB

Average RMS voltages and their relative reduction after applying artifact reduction methods are shown in table 1. Average RMS voltage was statistically significantly different between AAS + RLAS and AAS + RLAF (Wilcoxon rank sum test over channel RMS voltages, $p < 0.05$, average channel wise difference 1.4 μV, min/max difference 0.03 μV/19.82 μV). Average RMS voltage was statistically significantly different between AAS + RLAS and AAS + MBRLAF (Wilcoxon rank sum test over channel RMS voltages, $p < 0.01$, average channel wise difference 1.6 μV, min/max difference 0.12 μV/19.99 μV). No statistical difference was found between AAS + RLAF and AAS + MBRLAF. See figure 4 panel C.

Median RMS voltage attenuation of the applied artifact reduction methods are presented in table 2. RMS voltage reduction is given relative to the raw EEG RMS voltage. MBRLAF achieved the highest RMS voltage reduction of all methods. Artifact reduction for EEG channel FP1 of participant 1 was found to be low after any artifact reduction method and is marked as outlier in figure 4 panel D, but was not removed in analysis.

EEG signal power and artifact power are not evenly distributed over the frequency range. Table 3 and figure 5 show a complete overview of the powers per frequency band and their reduction per artifact reduction method. In terms of classical EEG frequency bands, the average power of artifact contaminated raw EEG data is starting at 300 μV^2 in the Delta band and reaches approx. 3.2×10^5 μV^2 in Gamma band. After artifact attenuation, average EEG power shows the opposite characteristic. Average EEG power is falling with frequency rising. Hence the average power difference of EEG data before and after artifact reduction is rising with frequency bands. The artifact reduction methods showed varying levels of success. The least average power reductions were achieved by AAS. RLAS achieved third lowest powers in all frequency bands except in the Gamma band. In the Gamma band, RLAS achieved second lowest power. RLAF achieved second lowest average power in any frequency band, accept in Gamma band. MBRALF artifact reduction achieved lowest average signal power in any classical EEG frequency band.

Alpha power topographies for the different artifact reduction methods are presented in figure 6. Alpha power topographies should show low and homogeneous alpha power at frontal and central electrode positions and high alpha power at

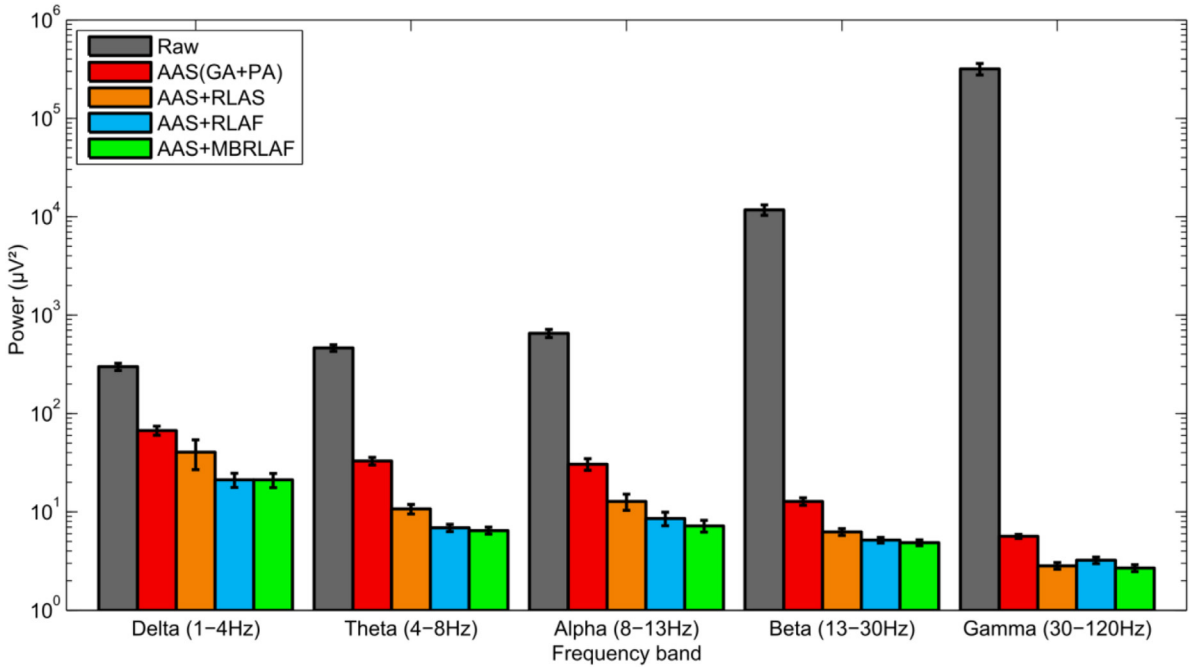

Figure 5. Average EEG power in common frequency bands. The average was computed over skin electrode signals before (Raw) and after artifact reduction. The error bars indicate standard error of the mean. Artifact reduction methods: average artifact subtraction of gradient artifact and pulse artifact (AAS of GA + PA), reference layer artifact subtraction (RLAS), reference layer adaptive filtering (RLAF), and multi band reference layer adaptive filtering (MBRLAF).

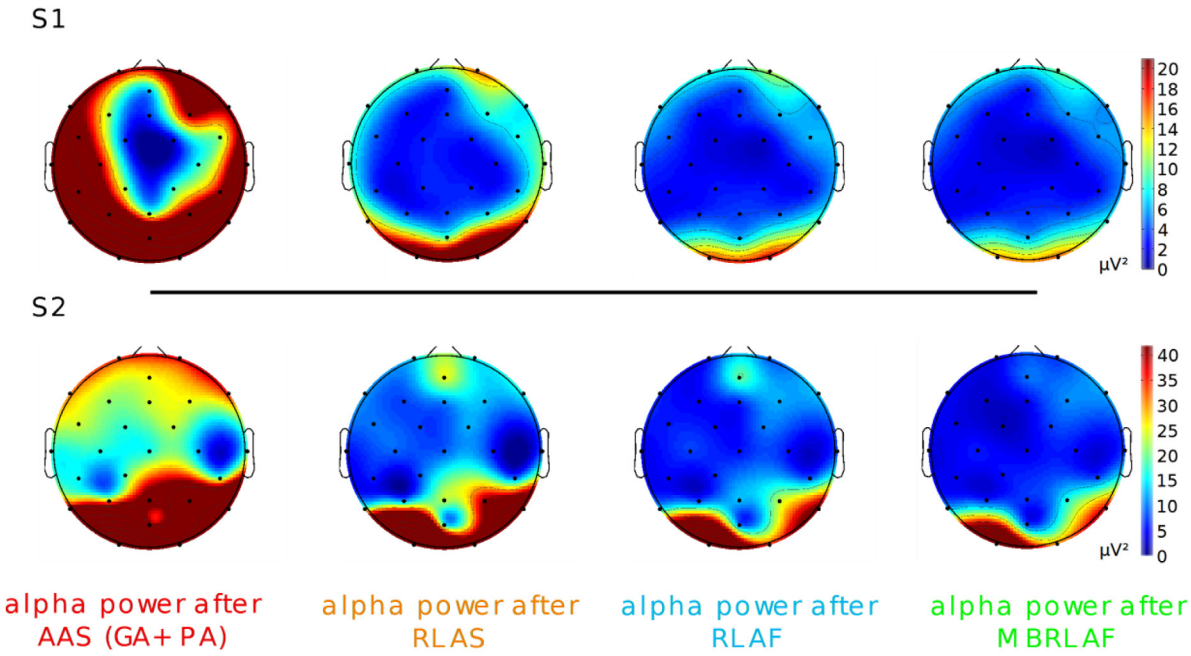

Figure 6. Average alpha power topographies during eyes closed for participant 1 (S1) and participant 2 (S2). Artifact reduction methods: average artifact subtraction of gradient artifact and pulse artifact (AAS of GA + PA), reference layer artifact subtraction (RLAS), reference layer adaptive filtering (RLAF), and multi band reference layer adaptive filtering (MBRLAF). Please note the different scaling for participant 1 and participant 2.

occipital electrode positions, when eyes are closed. The alpha power distribution after AAS is different. High alpha power at occipital positions is present, but also at frontal positions and for participant 1 also at lateral positions. In contrast, reference layer based approaches show a topography as expected. Low and homogeneous frontal and central alpha power and high occipital alpha power. For participant 1 some residuals are still visible after RLAS, particularly at lateral positions and frontal position FP2. The residuals are smaller after RLAF and MBRLAF. For participant 2 residuals at AFZ and P4 are visible after RLAS, and are smaller after RLAF and MBRLAF.

After artifact attenuation, the typical 1/*f* shape of EEG power spectra is visible and a classical EEG alpha peak is recognizable from 10 to 12 Hz. Moreover, artifactual spectral power

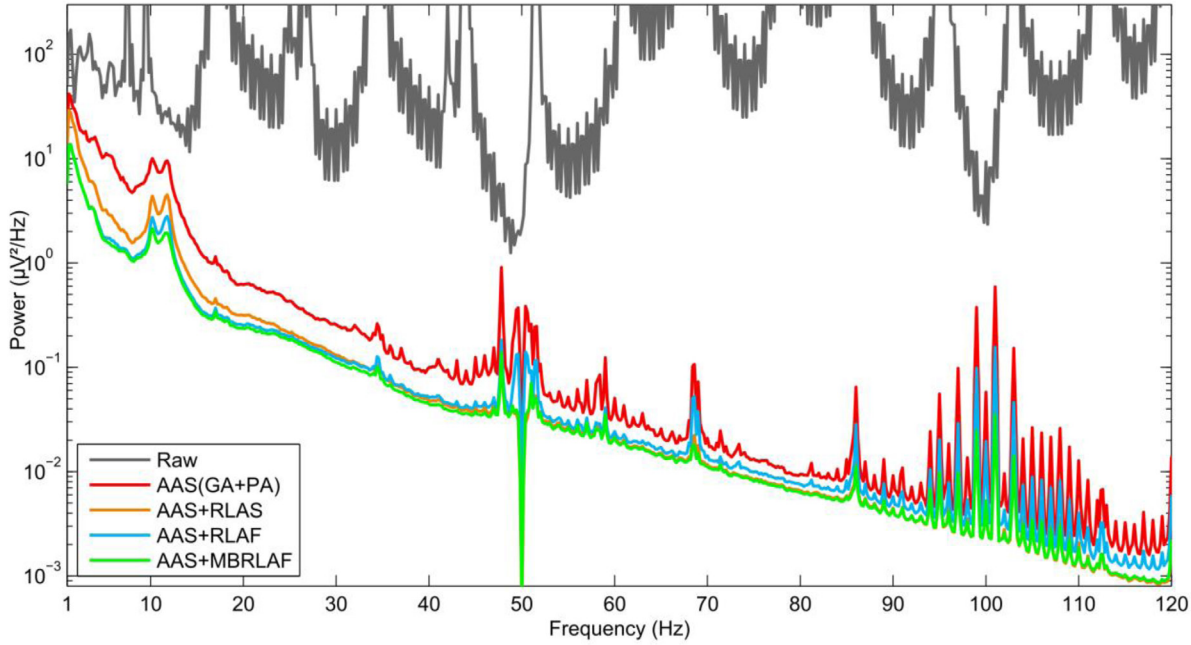

Figure 7. Average power spectra before (Raw) and after artifact reduction. Artifact reduction methods: average artifact subtraction of gradient artifact and pulse artifact (AAS of GA + PA), reference layer artifact subtraction (RLAS), reference layer adaptive filtering (RLAF), and multi band reference layer adaptive filtering (MBRLAF).

complexes are visible at around 17 Hz, 34.5 Hz, 47.8 Hz, 51.5 Hz, 59 Hz, 68.5 Hz, 86 Hz, 120 Hz, and a huge artifact complex of several peaks is ranging from 94 Hz to 113 Hz. Highest artifact power was found at 47.8 Hz with amplitudes of 0.91 $\mu V^2\,Hz^{-1}$, 0.15 $\mu V^2\,Hz^{-1}$, 0.18 $\mu V^2\,Hz^{-1}$, and 0.14 $\mu V^2\,Hz^{-1}$ after AAS, RLAS, RLAF, and MBRLAF, respectively. Highest power of the artifact complex at around 100 Hz was found at 101 Hz with amplitudes of 0.599 $\mu V^2\,Hz^{-1}$, 0.054 $\mu V^2\,Hz^{-1}$, 0.156 $\mu V^2\,Hz^{-1}$, and 0.035 $\mu V^2\,Hz^{-1}$ after applying AAS, RLAS, RLAF, and MBRLAF, respectively. Generally, reference layer methods achieved lower power per Hz than AAS. MBRLAF achieved the lowest power per Hz of all the methods within the total power spectrum. The power magnitude ranged from 1.4×10^{1} $\mu V^2\,Hz^{-1}$ at ~1 Hz to 8.6×10^{-4} $\mu V^2\,Hz^{-1}$ at ~119 Hz. RLAF achieved the second lowest power at low frequency ranges, but starting at ~35 Hz, RLAS achieved lower power than RLAF. Full power spectra are presented in figure 7.

Separate spectra of eyes open and eyes closed of both participants are presented in figure 8. A clear task specific change in the spectra is visible. Participant 1, depicted in figure 8 left panel, shows a classical increase in alpha power after eyes were closed. Participant 2, figure 8 right panel, shows a pronounced peak in alpha band already before eyes were closed, but alpha power increased further after eyes were closed. The spectral changes are more pronounced after MBRLAF.

The median of alpha power ratios between eyes closed and eyes opened was highest after MBRLAF (1.84), second highest after RLAF (1.80), third highest after RLAS (1.60), and lowest after AAS (1.37), see figure 9.

Specific VEP patterns were found for both participants and are shown in figures 10 and 11, respectively. For participant 1, highest VEP amplitudes were found at position O2. VEP homogeneity was measured in mean-squared-distance of single VEP to the respective average VEP at position O2. No specific VEP pattern was found at electrode position O1. For participant 2, highest VEP amplitudes were found at position O1. Mean-squared-distance (VEP homogeneity) of single VEPs to the corresponding average VEP were calculated at position O1. A similar VEP pattern, but with slightly lower amplitudes were found at electrode position O2. Table 4 summaries the maximum average VEP amplitudes and the mean-squared-distances to the average VEP.

Single trial VEP classification accuracies are presented in table 5. They were worst with raw EEG data and best after MBRLAF artifact reduction for both participants. For participant 1, classification accuracies ranged from a minimum of 52.8% to a maximum of 69.1%. For participant 2, accuracies ranged from a minimum of 54.2% to a maximum of 62.6%. Classification accuracies after AAS were higher than with raw EEG data, but never reached accuracies of reference artifact reduction methods. For participant 1, RLAF was the second best artifact reduction method while for participant 2 RLAS, RLAF and MBRLAF were practically equal.

Discussion

Reference layer cap prototype and EEG preprocessing

Our work represents a successful application of a truly reusable reference layer cap in combination with adaptive filtering to minimize residual artifacts in EEG of simultaneous EEG-fMRI in human. Our study extends and combines ideas for improving simultaneous EEG-fMRI data quality that were partly invented by work of Bonmassar *et al*, Masterton *et al* and the no longer available 'fEEG' system, and which were partly reinvestigated by a work of Chowdhury *et al*

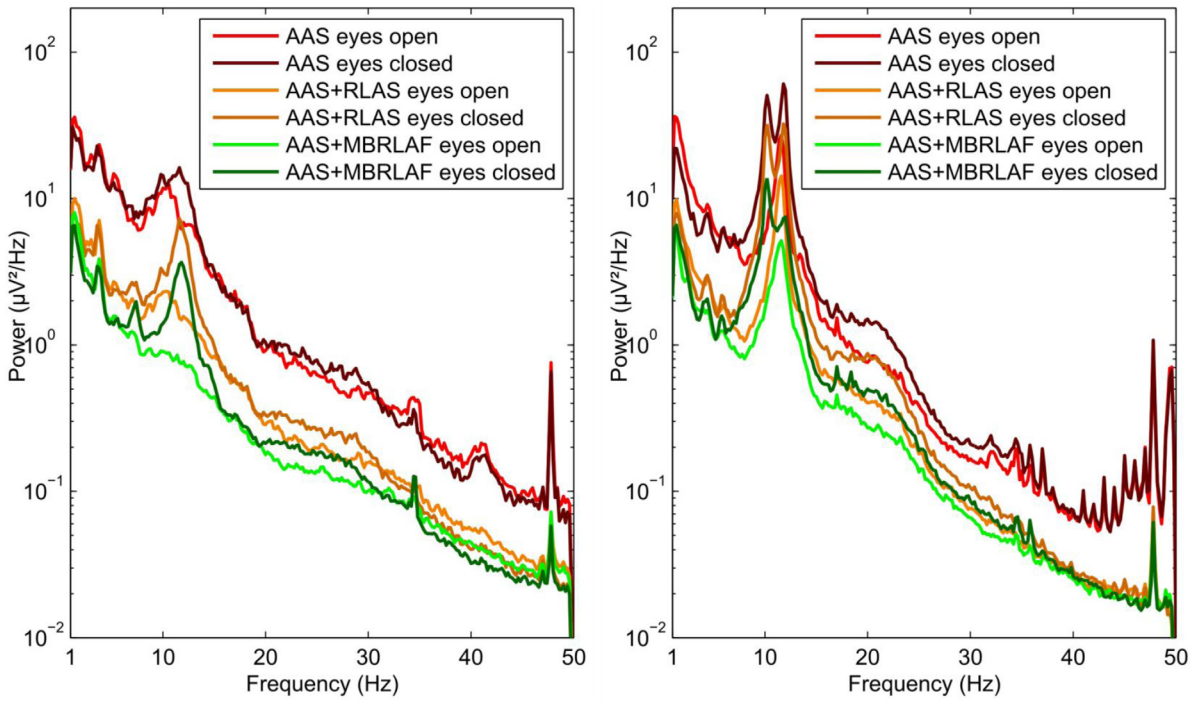

Figure 8. Power spectral density after average artifact subtraction (AAS), Reference layer artifact subtraction (RLAS), and multi band reference layer adaptive filtering (MBRLAF) of participant 1 (left panel) and participant 2 (right panel) averaged over occipital channels O1, O2, POZ, P3, P4, and PZ separately for eyes open and eyes closed.

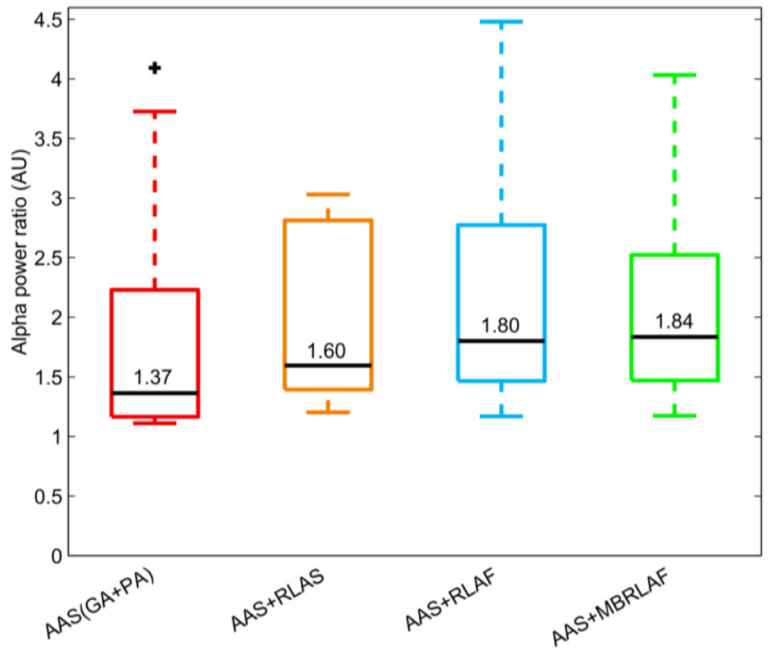

Figure 9. Alpha power ratios between eyes open and eyes closed after different artifact reduction methods at occipital channels O1, O2, POZ, P9, P3, PZ, PZ, P4, and P8. Higher is better. Artifact reduction methods: average artifact subtraction of gradient artifact and pulse artifact (AAS of GA + PA), reference layer artifact subtraction (RLAS), reference layer adaptive filtering (RLAF), and multi band reference layer adaptive filtering (MBRLAF).

(Bonmassar *et al* 2002, Masterton *et al* 2007, Dunseath *et al* 2009, Chowdhury *et al* 2014).

The reference layer cap prototype that we used in this work, is compatible with available fMRI capable EEG amplifier systems, which allows for an upgrade of systems that are already in use. Preparation and handling of the reference layer cap was similar to standard simultaneous EEG-fMRI caps in terms of duration as well as in terms of comfort for the participants. We did not notice additional susceptibility artifacts in visual inspections of fMRI images compared to standard simultaneous EEG-fMRI caps and EEG of reasonable quality became visible after AAS. The main benefit of this cap is, however, the

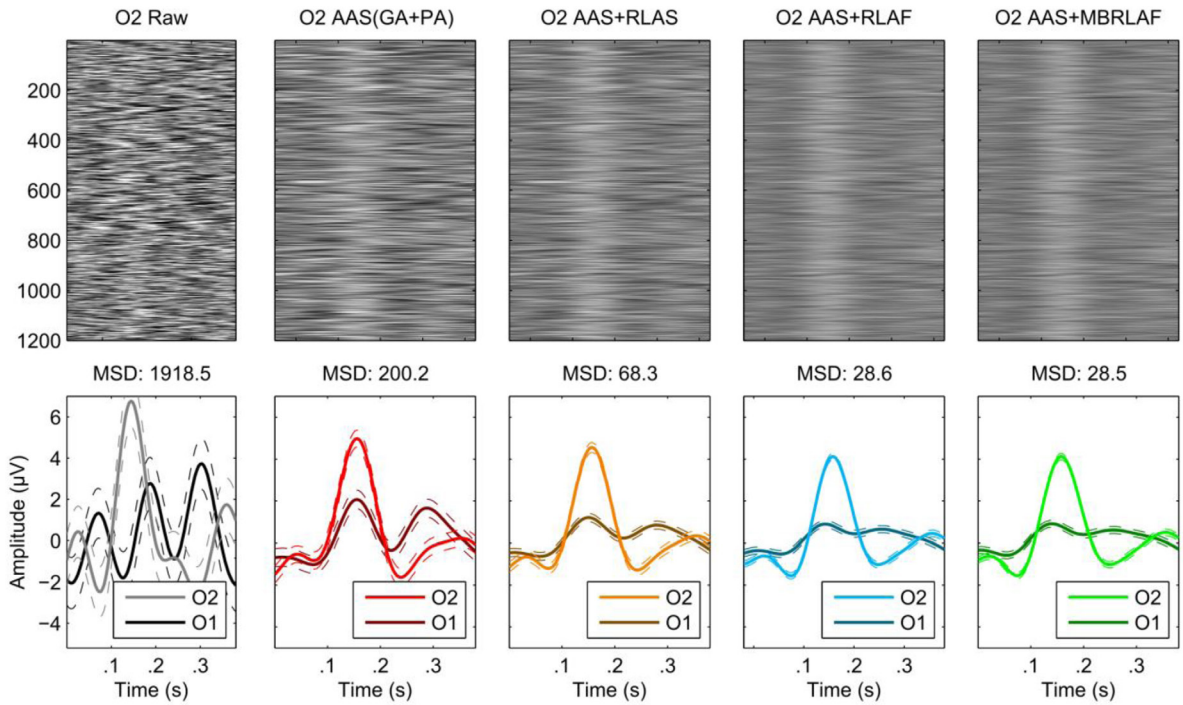

Figure 10. Visual evoked potentials (VEP) of participant 1. The upper row shows epochs of all recorded VEP at skin electrode O2 before (Raw) and after artifact reduction. Bottom row shows average VEP of skin electrodes of participant 1 at position O1 and O2. Dashed lines indicate standard error of the mean. The mean squared distance (MSD) of single VEP epochs to average VEP is a measure of VEP homogeneity and is exemplified in the middle row for participant 1 skin electrode position O2. Artifact reduction methods: average artifact subtraction of gradient artifact and pulse artifact (AAS of GA + PA), reference layer artifact subtraction (RLAS), reference layer adaptive filtering (RLAF), and multi band reference layer adaptive filtering (MBRLAF).

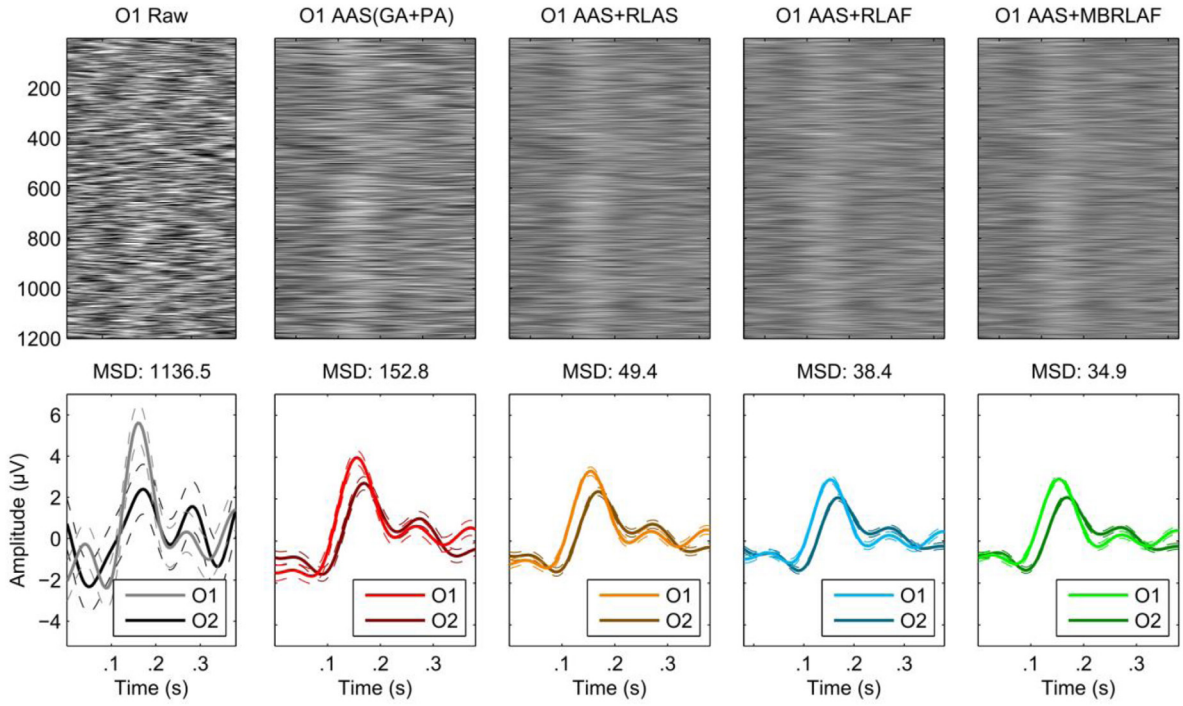

Figure 11. Visual evoked potentials (VEP) of participant 2. Upper row shows epochs of all recorded VEPs at skin electrode O1 before (Raw) and after artifact reduction. The bottom row shows average VEP of skin electrodes of participant 2 at position O1 and O2. Dashed lines indicate standard error of the mean. Mean squared distance (MSD) of single VEP epochs to average VEP is a measure of VEP homogeneity and is exemplified in the middle row for participant 2 skin electrode position O1. Artifact reduction methods: average artifact subtraction of gradient artifact and pulse artifact (AAS of GA + PA), reference layer artifact subtraction (RLAS), reference layer adaptive filtering (RLAF), and multi band reference layer adaptive filtering (MBRLAF).

Table 4. Maximum average VEP amplitudes per participant and per artifact correction method for EEG channels that showed the highest VEP amplitude. Mean-squared-distance of single VEPs to their respective average VEP. Mean-squared-distance is a measure for VEP homogeneity.

	Participant 1		Participant 2	
	Max VEP amp at O2 (μV)	MSD at O2 (μV^2)	Max VEP amp at O1 (μV)	MSD at O1 (μV^2)
Raw	6.7	1918.5	5.6	1136.5
AAS	5.0	200.2	4.0	152.8
AAS + RLAS	4.6	68.3	3.3	49.4
AAS + RLAF	4.1	28.6	2.9	38.4
AAS + MBRLAF	4.1	28.5	3.0	34.9

Table 5. Single trial visual evoked potential classification accuracies of participant 1 (S1) and participant 2 (S2) in percent before (Raw EEG) and after applying artifact reduction methods. Analytic shrinkage regularized linear discriminant analysis was applied in 100 repetitions of 5 fold cross-validation to estimate the accuracies and the standard deviations. Artifact reduction methods were: average artifact subtraction of gradient artifact and pulse artifact (AAS of GA + PA), reference layer artifact subtraction (RLAS), reference layer adaptive filtering (RLAF), and multi band reference layer adaptive filtering (MBRLAF).

ID	Raw EEG (%)	AAS(GA + PA) (%)	AAS + RLAS (%)	AAS + RLAF (%)	AAS + MBRLAF (%)
S1	52.8 ± 2.3	57.0 ± 2.2	62.1 ± 2.3	68.4 ± 2.1	69.1 ± 2.1
S2	54.2 ± 2.3	58.8 ± 2.2	61.7 ± 2.1	61.5 ± 2.2	62.6 ± 2.0

optional use of reference layer based approaches to improve EEG quality further, namely RLAS and the two methods that we introduced with this work, RLAF and MBRLAF. Visual inspection of EEG after applying artifact reduction methods indicate the benefits of reference layer based approaches, namely reducing residual artifacts, while preserving physiological EEG components. We found that MBLRAF reduces artifact components most, followed by RLAF and RLAS.

Preprocessing is crucial for the efficacy of reference layer based approaches. Our experience within this work support the findings of Chowdhury *et al* and Jorge *et al* about the sequence when combining AAS and RLAS (Chowdhury *et al* 2014, Jorge *et al* 2015b). AAS before RLAS was most effective, while altering the pre-processing sequence impaired the efficacy of RLAS. We observed a similar behavior with RLAF and MBRLAF.

RLAS

In line with Chowdhury *et al* and Jorge *et al* we observed reduced residual artifacts in visual inspections of EEG data after applying RLAS, while physiological EEG activity was preserved (Chowdhury *et al* 2014, Jorge *et al* 2015b). In the present work, RLAS achieved an overall RMS voltage reduction of −37.8 dB compared to the Raw EEG, which is an improvement over AAS by −5.1 dB. Average power in common EEG frequency bands was lower after RLAS than after AAS. Topographical plots of alpha power during eyes closed show reduced residual artifacts at frontal and lateral electrode positions after RLAS compared to AAS. RLAS was also effective in reducing artifacts in higher frequency bands, as visible in the full power spectrum. Further, higher median alpha power ratios as well as more pronounced VEPs with smaller MSD to the average VEP, indicate the preservation of physiological EEG components and underlines the effectiveness of RLAS. However, as mentioned in the introduction, there are several causes why artifacts at the reference layer can be different from artifacts at scalp, which implies that a straightforward subtraction of reference layer signals from scalp layer signals, as applied in RLAS, might be improved. Practically observed scaling values of the adaptive filters demonstrate that for optimal (in the LMS sense) artifact attenuation reference layer signals need to be scaled by factors between ~0.5 and ~2. Theoretical considerations based on Faraday's law justify a linear relationship assumption between reference and scalp layer artifacts, although, the linear relationship can change over time, for example due to motion or due to changes in electrode impedances (Jorge *et al* 2015b). The time courses of the adaptive filters scaling factors provide evidence for that assumption. We perceived three prototypical courses of scaling factors: (i) no change in scaling factors over time. The linear approximation of our example in figure 3 showed practically no change over time with scaling factors of 0.7 in the beginning and in the end. (ii) Linear change over time. In our example the scaling factors increased from 1.2 to 1.4, which is a relative change of 16.7% over ~20 min. We assume that slow drifts in the electrode impedances are the cause for that changes. (iii) Abrupt change in scaling factors. We perceived that the scaling factors can also change abrupt, in our example from 1.7 to 2.0. That is a relative change of ~18%. We attribute this fast changes to slight motions which change the orientation of the electrodes and therefore the relationship between the scalp and reference electrode. Motions can also change the pressure on electrodes and therefore the impedance. Particularly time courses like (ii) and (iii) are problematic when the scaling factors are time invariant. Errors of up to 20% can be introduces within 20 min. The problems of changing impedances and of motion were for example already brought up in Masterton *et al* (2007) and Jorge *et al* (2015b). The theoretical considerations, combined

with our practical experiences with RLAS and the aforementioned discussions give the justification why we replaced subtraction by adaptive filtering in our RLAF approach.

Reference layer adaptive filtering (RLAF)

Any artifact reduction in simultaneous EEG-fMRI experiments is highly appreciated, since it is still challenging to achieve high EEG quality in these experiments, which in turn is a necessity for a broader field of application of simultaneous EEG-fMRI. Within our work, we found adaptive filtering potentially superior to straight forward subtraction. Visual inspection of EEG after RLAF artifact reduction shows mitigated residual artifacts compared to EEG after RLAS. Residual artifacts after RLAF are visually hardly noticeable. RLAF outperforms RLAS in terms of RMS voltage reduction, while maintaining physiological signals. RLAF achieved significantly lower RMS voltages compared to RLAS (on average 16.5% lower), which is equal to 1.6 dB lower median power when analyzing the full bandwidth EEG. The computational effort of the RLAF approach is easily manageable. One adaptive filter per electrode pair, hence 29 in our experiment, is not at all a problem for modern computers. Back in 2007 Masterton *et al* used already more complex adaptive filters (Masterton *et al* 2007). Hence, an online application is conceivable.

Adaptive filters commonly take into account current and past samples of a signal. The number of past samples is reflected by the model order of the adaptive filter and represent a learned and adaptively tuned FIR filter (Haykin 1986, Shynk 1992). We chose a first order model which restricts an adaptive filter to adaptive scaling of the current sample. One can argue that a higher order model would be beneficial since the optimal filter would be learned too. However, preliminary unpublished investigations by ourselves suggests that higher order models have only a marginal effect. We attribute that behavior to the combination of the LMS optimization criterion of our adaptive filters and the spectral power distribution of EEG. LMS adaptive filters aim to minimize the overall residual power after filtering. Most EEG power is present in low frequency ranges and less power in higher frequency ranges, which is well known as $1/f$ characteristic. Hence, adaptive filters find an optimal scaling for the lower frequency components since lower frequency components contribute most to the overall residuals. Adaptive filters with higher order models, still have the same LMS optimization criterion and still most power is present in lower frequency bands. Hence, we experienced that a low pass filter is learned and the adaptive filter again optimizes the scaling for low frequency ranges, which only marginally improved the adaptive filter quality compared to the first order model.

An EEG power analysis per frequency band indicate that RLAF potentially outperforms RLAS from Delta to Beta band, but is less effective in the Gamma band. This behavior is also visible in the full spectra. RLAF achieves lower power than RLAS up to ~35 Hz, but in higher frequency ranges, RLAF is less effective than RLAS. This is a consequence of the aforementioned adaptation of the scalings to lower frequency ranges because of their higher power.

The topological alpha power plots show lower residual artifacts after applying RLAF when compared to topo plots after RLAS. Particularly frontal channels can benefit from RLAS. Higher median alpha power ratios as well as VEPs with small MSD to the average VEP, indicate the preservation of physiological EEG components and also indicate a higher effectiveness of RLAF compared to RLAS. All together, these results point at a potentially improved effectiveness of RLAF over RLAS, at least in lower frequency ranges of up to ~35 Hz.

Multi band reference layer adaptive filtering (MBRLAF)

We enhanced the RLAF approach by restricting the frequency range of reference and scalp signals to multiple sub-bands and performed a separate adaptive filtering per sub-band (Shynk 1992). Therefore, we named this approach MBRLAF. As a consequence of the frequency range restriction to sub-bands, each adaptive filter minimized the LMS residuals separately for each band. This resulted in a method that achieves lowest RMS voltages over all, but also lowest power over the whole frequency range and was the best performing method over all. MBRLAF achieved significantly lower RMS voltages compared to RLAS, on average 18.8% lower and achieved also lower RMS voltages than RLAF. However, the reduction of power distribution dependency comes at the cost of computation power. A lot more adaptive filters are necessary (one per sub-band) and computational cost increases linearly with the number of adaptive filters. Luckily, the adaptive filtering can be parallelized on channel level, hence, a real time application of a modified MBRLAF algorithm is conceivable in future. The improvement of MBRLAF over RLAS is significantly, however, the improvement over RLAF is rather marginally, on average 0.2 μV less RMS voltage. Topological alpha power plots are comparable to RLAF, maybe with a small advantage for MBRLAF. MBRLAF achieved in median the highest alpha power ratio between eyes closed and eyes open and the lowest MSD of single VEPs to the average VEP. These potentially higher effectiveness of MBRLAF is particularly important in higher frequency ranges where signals of interest are already very small and where every possible improvement in signal quality is very welcome.

Preservation of physiological components in the EEG

Reductions in RMS voltage and EEG power are characteristics for artifact reduction only if physiological components are not removed from EEG. Four facts indicate that reference layer based methods preserve physiological components. (i) The shape of EEG spectra: a $1/f$ decay in EEG spectral power is clearly visible after all artifact reduction methods (Schomer and da Silva 2011). (ii) A peak in spectral power at 10 Hz to 12 Hz, the alpha peak, is also clearly visible (Schomer and da Silva 2011). (iii) The dedicated spectra and also the alpha power ratios demonstrate that occipital alpha power is increasing with eyes closed compared to eyes opened, as it

is expected (Schomer and da Silva 2011). The alpha power ratios are higher with reference layer based approaches, indicating better preservation. (iv) VEPs are preserved and average VEPs are very similar after applying different artifact reduction methods (Schomer and da Silva 2011). Hence, a removal of evoked potentials can be ruled out. Concluding these four facts, we do not see a removal of physiological EEG components.

Evoked potentials quality improvement and practical implications

Mean-squared-distance of single evoked potentials to their respective average evoked potential is a measure of variance in EEG that is not related to evoked potentials. This variance consists of ongoing, spontaneous EEG and artifacts. One wants of course to reduce exclusively artifacts. However, when reduced MSD measures are computed, one cannot distinguish which of these two components was removed. Nevertheless, we found induced activity (alpha peak) which is in coincidence with eyes open and eyes closed episodes, and indicate that artifacts were reduced and not ongoing EEG. Hence, a low MSD of evoked potentials to their average evoked potential implies a reduction in artefacts. RLAF and MBRLAF are both capable to reduce the MSD by up to 58% compared to RLAS.

EEG quality improvement has practical implications for simultaneous EEG-fMRI experiments. An improved VEP homogeneity directly impacts experimental design, since a lower number of VEPs is necessary for the same quality of average VEPs. The experiments can thus be of shorter duration, which in turn is beneficial to avoid tiredness of study participants. On single trial level, VEPs are more pronounced. Single trial classification of VEPs benefit as well from MBRLAF. In our single trial accuracy estimation via cross validation, we obtained highest average classification accuracies after MBRLAF. Classification accuracies of participant 1 improved up to 12% from baseline (AAS). Classification accuracies of participant 2 were practically identical after RLAS, RLAF and MBRLAF, which implies only marginal improvement, but indicates that no information, hence VEP, was removed. Classification accuracy is important in many experiments for the accurate detection of brain patterns (Lotte *et al* 2007, Steyrl *et al* 2016).

Limitations

By concept this setup needs two EEG channels per later-to-be-derived EEG signal. For example, a 64 channel setup is necessary to bring the later-to-be-derived channel count to 32. With currently available hardware, 128 or even higher numbers of channels are possible, but comes with the caveat of introducing more technical equipment into the scanner bore, which can be impractical. However, we assume that this caveat should become less important in future, since the number of available channels in EEG hardware steadily increased over the past years. Further we are aware of many experiments where high quality EEG is more important than the pure number of channels, especially when it comes to analysis of brain signals with a very bad signal-to-noise-ratio, like it is the case for gamma band activity.

In addition to these conceptual limitations, we also perceived practical restrictions. Although no major problems arose during the actual use of the reference layer cap prototype, we found the durability of the silver coated electrodes limited over the long term. The abrasive gel removed the silver coating, which made the cap unusable after several measurements. Future caps need to be equipped with sintered Ag/AgCl pellets, which are more robust (Schomer and da Silva 2011).

The RLAF/MBRLAF approach should in principle be able to cope with motion artifacts, since this was shown already for the RLAS approach by Chowdhury *et al* and we further improved the motion dependent behavior by using the mechanically tightly coupled electrode pair (Chowdhury *et al* 2014). We, however, did not test for these artifacts explicitly in this work. This is future work.

And finally, although EEG quality was improved, residual artifacts are still present after applying AAS, RLAS, RLAF, or MBRLAF. The spectra show remaining artifacts of non-negligible magnitudes. Particularly the huge artifact complex at about 100 Hz is prominent, which is presumably caused by the helium pump. However, it is not yet clear why this artifact is still present after the application of RLAF or MBRLAF. We speculate that more than one source emits interfering electromagnetic fields which are not in phase and therefore the adaptive filter is not able to find a scaling that eliminates this artifact. For illustration, if the adaptive filter finds a scaling that removes one part of the artifact, the other is still present and vice versa, although both components are present in the reference layer. However, this artifact will need further investigations.

Summary

We showed that, based on theoretical considerations, there is potential to increase EEG quality by combining a reference layer with adaptive filtering. We brought practical evidence that EEG quality is potentially improved after applying RLAF or MBRLAF compared to previous methods. We observed reduced artifacts in visual inspections of EEG data after RLAF or MBRLAF artifact reduction. RMS voltage and spectral power were reduced, while physiological EEG components were preserved, even when the coolant system of the scanner was active. RLAF was effective in reducing artifact components up to ~35 Hz, while MBRLAF was the most effective method in all frequency ranges. Nevertheless, residual artifact components above 40 Hz are still present and must be kept in mind when analyzing simultaneous EEG-fMRI data.

In conclusion, we see RLAF and MBRLAF as a potential step forwards to the goal of achieving high quality EEG in simultaneous EEG-fMRI measurements over the full frequency range and particularly for high EEG quality in classical EEG frequency ranges.

Acknowledgments

This work was partly supported by the ERC Consolidator Grant 681231 'Feel Your Reach'. The authors wish to thank Martin Seeber and Prof. Hermann Scharfetter for fruitful discussion and comments.

References

Abbott D F, Masterton R A J, Archer J S, Fleming S W, Warren A E L and Jackson G D 2014 Constructing carbon fiber motion-detection loops for simultaneous EEG–fMRI *Front. Neurol.* **5** 260

Abolghasemi V and Ferdowsi S 2015 EEG–fMRI: dictionary learning for removal of ballistocardiogram artifact from EEG *Biomed. Signal Process. Control* **18** 186–94

Abreu R, Leite M, Jorge J, Grouiller F, van der Zwaag W, Leal A and Figueiredo P 2016 Ballistocardiogram artefact correction taking into account physiological signal preservation in simultaneous EEG-fMRI *NeuroImage* **15** 45–63

Acharjee P P, Phlypo R, Wu L, Calhoun V D and Adali T 2015 Independent vector analysis for gradient artifact removal in concurrent EEG-fMRI Data *IEEE Trans. Biomed. Eng.* **62** 1750–8

Allen P J, Josephs O and Turner R 2000 A method for removing imaging artifact from continuous EEG recorded during functional MRI *NeuroImage* **12** 230–9

Allen P J, Polizzi G, Krakow K, Fish D R and Lemieux L 1998 Identification of EEG events in the MR scanner: the problem of pulse artifact and a method for its subtraction *NeuroImage* **8** 229–39

Blankertz B, Lemm S, Treder M, Haufe S and Müller K-R 2011 Single-trial analysis and classification of erp components—a tutorial *NeuroImage* **56** 814–25

Bonmassar G, Hadjikhani N, Ives J R, Hinton D and Belliveau J W 2001 Influence of EEG electrodes on the BOLD fMRI signal *Hum. Brain Mapp.* **14** 108–15

Bonmassar G, Purdon P L, Jääskeläinen I P, Chiappa K, Solo V, Brown E N and Belliveau J W, 2002 Motion and ballistocardiogram artifact removal for interleaved recording of EEG and EPs during MRI *NeuroImage* **16** 1127–41

Briselli E, Garreffa G, Bianchi L, Bianciardi M, Macaluso E, Abbafati M, Marciani M G and Maraviglia B 2006 An independent component analysis-based approach on ballistocardiogram artifact removing *Magn. Reson. Imaging* **24** 393–400

Brookes M J, Mullinger K J, Stevenson C M, Morris P G and Bowtell R 2008 Simultaneous EEG source localisation and artifact rejection during concurrent fMRI by means of spatial filtering *NeuroImage* **40** 1090–104

Chowdhury M E, Mullinger K J, Glover P and Bowtell R 2014 Reference layer artefact subtraction (RLAS): a novel method of minimizing EEG artefacts during simultaneous fMRI *NeuroImage* **84** 307–19

Debener S, Mullinger K J, Niazy R K and Bowtell R W 2008 Properties of the ballistocardiogram artefact as revealed by EEG recordings at 1.5, 3 and 7 tesla static magnetic field strength *Int. J. Psychophysiol.* **67** 189–99

Debener S, Strobel A, Sorger B, Peters J, Kranczioch C and Engel A K 2007 Improved quality of auditory event-related potentials recorded simultaneously with 3 T fMRI: removal of the ballistocardiogram artefact *NeuroImage* **34** 587–97

Dunseath W J R and Alden T A 2009 Electrode Cap for Obtaining Electrophysiological Measurement Signals from Head of Subject, has Measurement Signal Electrodes Extended through Electrically Conductive Layer and Insulating Layer for Contacting Head of Subject *US Patent Specification* 2009/0099473 USA

Ferdowsi S, Sanei S, Abolghasemi V, Nottage J and O'Daly O 2013 Removing Ballistocardiogram artifact from EEG using short- and long-term linear predictor *IEEE Trans. Biomed. Eng.* **60** 1900–11

Haykin S 1986 *Adaptive Filter Theory* 5th edn (Englewood Cliffs, NJ: Prentice-Hall)

He B, Yang L, Wilke C and Yuan H 2011 Electrophysiological imaging of brain activity and connectivity—challenges and opportunities *IEEE Trans. Biomed. Eng.* **58** 1918–31

Huster R J, Debener S, Eichele T and Herrmann C S 2012 Methods for simultaneous EEG-fMRI: an introductory review *J. Neurosci.* **32** 6053–60

Jorge J, Grouiller F, Gruetter R, van der Zwaag W and Figueiredo P 2015b Towards high-quality simultaneous EEG-fMRI at 7 T: detection and reduction of EEG artifacts due to head motion *NeuroImage* **120** 143–53

Jorge J, Grouiller F, Ipek Ö, Stoermer R, Michel C M, Figueiredo P, van der Zwaag W and Gruetter R 2015a Simultaneous EEG-fMRI at ultra-high field: artifact prevention and safety assessment *NeuroImage* **105** 132–44

Laufs H 2012 A personalized history of EEG–fMRI integration *NeuroImage* **62** 1056–67

Liu Z, de Zwart J A, Van Gelderen P, Kuo L W and Duyn J H 2012 Statistical feature extraction for artifact removal from concurrent fMRI-EEG recordings *NeuroImage* **59** 2073–87

Lotte F, Congedo M, Lécuyer A, Lamarche F and Arnaldi B 2007 A review of classification algorithms for EEG-based brain-computer interfaces *J. Neural. Eng.* **4** 1–13

Luo Q and Glover G H 2012 Influence of dense-array EEG cap on fMRI signal *Magn. Reson. Med.* **68** 807–15

Luo Q, Huang X and Glover G H 2014 Ballistocardiogram artifact removal with a reference layer and standard EEG cap *J. Neurosci. Methods* **233** 137–49

Mantini D, Perrucci M G, Cugini S, Ferretti A, Romani G L and Del Gratta C 2007 Complete artifact removal for EEG recorded during continuous fMRI using independent component analysis *NeuroImage* **34** 598–607

Masterton R A, Abbott D F, Fleming S W and Jackson G D 2007 Measurement and reduction of motion and ballistocardiogram artefacts from simultaneous EEG and fMRI recordings *NeuroImage* **37** 202–11

McGlone F, Dunseath R and Stern J 2009 Simultaneous EEG and functional MRI employing novel noise reduction *Epilepsia* **50** 82–2

Michel C M and Murray M M 2012 Towards the utilization of EEG as a brain imaging tool *NeuroImage* **61** 371–85

Mulert C and Lemieux L 2010 *EEG-fMRI Physiological Basics, Technique, and Applications* (Heidelberg: Springer)

Mullinger K J and Bowtell R 2011 Combining EEG and fMRI ed M Modo and J W M Bulte *Magnetic Resonance Neuroimaging, Methods in Molecular Biology* vol 711 (Springer) pp 303–26

Mullinger K J, Castellone P and Richard Bowtell R 2013b Best current practice for obtaining high quality EEG data during simultaneous fMRI *J. Vis. Exp.* **76** 50283

Mullinger K J, Havenhand J and Bowtell R 2013a Identifying the sources of the pulse artefact in EEG recordings made inside an MR scanner *NeuroImage* **7** 75–83

Mullinger K J, Morgan P S and Bowtell R W 2008 Improved artifact correction for combined electroencephalography/functional mri by means of synchronization and use of vectorcardiogram recordings *J. Mag. Res. Imaging* **27** 607–16

Mullinger K J, Yan W X and Bowtell R 2011 Reducing the gradient artefact in simultaneous EEG-fMRI by adjusting the subject's axial position *NeuroImage* **54** 1942–50

Niazy R K, Beckmann C F, Iannetti G D, Brady J M and Smith S M 2005 Removal of FMRI environment artifacts from EEG data using optimal basis sets *NeuroImage* **28** 720–37

Niedermeyer E and Lopes da Silva F H 2005 *Electroencephalography: Basic Principles, Clinical Applications, and Related Fields* 5th edn (Philadelphia: Williams & Wilkins)

Nierhaus T, Gundlach C, Goltz D, Thiel S D, Pleger B and Villringer A 2013 Internal ventilation system of MR scanners induces specific EEG artifact during simultaneous EEG-fMRI *NeuroImage* **74** 70–6

Norris D G 2006 Principles of magnetic resonance assessment of brain function *J. Magn. Reson. Imaging* **23** 794–807

Ogawa S, Lee T M, Kay A R and Tank D W 1990 Brain magnetic resonance imaging with contrast dependent on blood oxygenation *Proc. Natl Acad. Sci. USA* **87** 9868–72

Ritter P and Villringer A 2006 Simultaneous EEG-fMRI *Neurosci. Biobehav. Rev.* **30** 823–38

Ritter P, Becker R, Graefe C and Villringer A 2007 Evaluating gradient artifact correction of EEG data acquired simultaneously with fMRI *Mag. Res. Imaging* **25** 923–32

Rothlübbers S, Relvas V, Leal A, Murta T, Lemieux L and Figueiredo P 2014 Characterisation and reduction of the EEG artefact caused by the helium cooling pump in the MR environment: validation in epilepsy patient data *Brain Topogr.* **28** 208–20

Schomer D L and da Silva F L 2011 *Niedermeyer's Electroencephalography: Basic Principles, Clinical Applications and Related Fields* (Philadelphia: Williams & Wilkins)

Shynk J J 1992 Frequency-domain and multirate adaptive filtering *IEEE Signal Process. Mag.* **9** 14–37

Srivastava G, Crottaz-Herbette S, Lau K M, Glover G H and Menon V 2005 ICA-based procedures for removing ballistocardiogram artifacts from EEG data acquired in the MRI scanner *NeuroImage* **24** 50–60

Steyrl D, Patz F, Krausz G, Edlinger G and Müller-Putz G R 2015 Reduction of EEG artifacts in simultaneous EEG-fMRI: reference layer adaptive filtering (RLAF) *2015 37th Annual Int. Conf. of the IEEE Engineering in Medicine and Biology Society (EMBC)* pp 3803–6

Steyrl D, Scherer R, Faller J and Müller-Putz G R 2016 Random forests in non-invasive sensorimotor rhythm brain-computer interfaces: a practical and convenient non-linear classifier *Biomed. Eng.-Biomed. Tech.* **61** 77–86

Uludag K and Roebroeck A 2014 General overview on the merits of multimodal neuroimaging data fusion *NeuroImage* **102** 3–10

van der Meer A P, Van Someren E J W, Ramautar J R, van der Werf Y D, Gomez-Herrero G, Lepsien J, Hellrung L, Hinrichs H, Möller H E and Martin Walter M 2016 Carbon-wire loop based artifact correction outperforms post-processing EEG/fMRI corrections-a validation of a real-time simultaneous EEG/fMRI correction method *NeuroImage* **125** 880–94

van der Meer J N, Tijssen M A J, Bour L J, Van Rootselaar A F and Nederveen A J 2010 Robust EMG–fMRI artifact reduction for motion (FARM) *Clin. Neurophysiol.* **121** 766–76

Vanderperren K *et al* 2010 Removal of BCG artifacts from EEG recordings inside the MR scanner: a comparison of methodological and validation-related aspects *NeuroImage* **50** 920–34

Wu X, Wu T, Zhan Z, Yao L and Wen X 2016 A real-time method to reduce ballistocardiogram artifacts from EEG during fMRI based on optimal basis sets (OBS) *Comput. Methods Programs Biomed.* **127** 114–25

Xia H, Ruan D and Cohen M S 2013 BCG Artifact removal for reconstructing full-scalp EEG inside the MR scanner *2013 Int. Workshop on Pattern Recognition in Neuroimaging (PRNI)* pp 178–81

Yan W X, Mullinger K J, Geirsdottir G B and Bowtell R 2010 Physical modeling of pulse artefact sources in simultaneous EEG/fMRI *Hum. Brain Mapp.* **31** 604–20